Summary Report

On

Design, development and characterization of phthalocyanine nanostructures for biosensing and drug delivery in diabetes

To be submitted

to

Research and Recognition Committee

of

Ph.D. Programme

In

Pharmaceutical Sciences

Candidate

Ms. Sharayu Govardhane

Supervisor

Dr. Pravin K. Shende

Registration date: 5th December, 2020

Summary Report

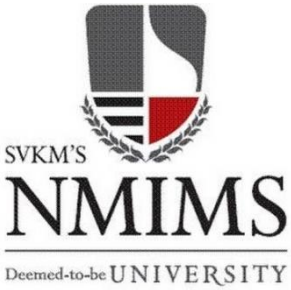

Shobhaben Pratapbhai Patel

School of Pharmacy and Technology Management

SVKM's Narsee Monjee Institute of Management Studies,

V.L. Mehta Road, Vile Parle (W), Mumbai-400056

TITLE: Design, development and characterization of phthalocyanine nanostructures for biosensing and drug delivery in diabetes

1. Introduction

Diabetes mellitus is a metabolic disorder that causes increase in sugar (glucose) level in the blood rather than being used as energy by the cells in our body [1]. When diet is consumed, it is fragmented down by digestive enzymes into nutrient complexes which are then absorbed by the digestive system. Glucose is the main source of energy for the cells, tissues and organs of the cells in the pancreas and required for penetration into the cells. According to the International Diabetes Federation, the global diabetes prevalence in 2019 was estimated to be 9.3% (463 million people), rising to 10.2% (578 million) by 2030 and 10.9% (700 million) by 2045. In diabetes, β-cells of pancreas are incapable to produce an adequate amount of insulin to prevent hyperglycemic conditions [2].

Diabetes mellitus may occur from interaction between genetic, environmental and other factors like dietary intake, exercise, sedentariness, sleep and stress. People suffering from diabetes are vulnerable to various health-related problems, which may lead to early death [3]. No specific remedy has yet been found for the disorder; however, therapy modalities include routine alterations in life-style, reduction in obese conditions, hypoglycemic agents, and insulin sensitizers like metformin, a class of biguanide that decreases the insulin resistance, however, is still considered as a first-line treatment specifically in over-weight patients. Oxidative stress leads to the production of reactive oxygen species (ROS) and has been proposed as the root cause for the development of insulin resistance, β-cell dysfunction, impaired glucose tolerance and diabetes mellitus [4].

About one in four people suffering from diabetes are unacquainted that they are suffering from the disease. It is important to detect diabetes early because over time high blood glucose

damages the blood vessels creating various health complications like kidney damage, skin conditions, cardiovascular diseases, etc. Early detection and treatment are the important steps towards keeping people healthy from diabetes. It can help to reduce the risk of serious complications such as premature heart disease and stroke, blindness, limb amputations and kidney failure. There are different technique considered for diagnosis of diabetes such as random blood sugar test, fasting blood sugar test, oral glucose tolerance test, etc. [6]. There is a need of a convenient, non-invasive, sensitive and accurate diagnostic tool for the estimation of glucose. [7].

Phthalocyanine is an important dye with numerous applications in the fields of biological, photophysical, and analytical and characterized for its high hydrophobicity and self-aggregation tendency in aqueous media, which hamper its potential application [8]. Phthalocyanine is reported to show the ability to prevent the initiation of a peroxidative chain reaction and slowing down the progression of a peroxidative chain reaction. Phthalocyanine emerges in the treatment of various conditions such as cancer, bacterial infections, wound healing process, etc. Phthalocyanine functionalize the recoupling of eNOS (endothelial nitric oxide synthase), thus leading to increase in vascular NADPH (nicotinamide adenine dinucleotide phosphate oxidase) activity. This helps against the development of diabetes by inhibiting formation of reactive oxygen stress/ scavenge free radicals generation and thus suppressing the activity lipid peroxidation [9].

Metal nanostructures (NPs) exhibit different properties from bulk metal due to quantum size effects, including novel electronic, optical and chemical behaviour. The properties may be tuned by controlling the size, shape inter-particle spacing and dielectric environment, and methods. The recent studies displayed that zinc oxide-nanoparticles reduces blood glucose levels in diabetic animals [10].

Amongst, the various lipid formulations, liposomal formulation is considered as primary lipid formulation which consists of phospholipid (major component on biological membrane) and used for diabetes management [11]. Lipoplexes, another lipid-based assembly consisting of non-covalently associated DNA by charge-charge interactions, have recently used in the treatment of diabetes. Encapsulation of phthalocyanine in the lipid nanoparticles may help in increasing the solubility and thus, enhancing the penetration of nanoparticles inside the cell [12].

Polymeric nanostructures are sub-micron colloidal structures consisting of active entrapped within or adsorbed to polymeric molecules. Polymeric nanostructures showed their advantage by revolutionary change to produce new biomaterials with tailored properties and functionalities for targeted biomedical applications such as protein, peptide, DNA, RNA delivery, etc. [13].

2. Approach to the issue

Although there are many therapies available for the treatment of diabetes, but no complete cure is possible. Among many techniques available for the diagnosis of diabetic, invasive and instrumental methods are used for the detection. Diagnosis of diabetes from the exhaled air via mouth will be a non-invasive and easy technique, thus helping in early detection and treatment. Phthalocynine is a hydrophobic macromolecule, thus limiting its application for the treatment of diabetes. As metal shows insulin-mimicking ability, the conjugation of phthalocynine with the metal will increase the therapeutic in diabetes. Whereas the conjugation of phthalocynine with the lipid will increase the penetration ability of the drug inside the infected cell, thus increases the bioavailability of the drug and maintains the volume of distribution in the body. The conjugation of phthalocynine along with the polymer will help in the site-specific delivery along with an increase in bioavailability.

6. Objective of work

i. Diagnosis

To develop exhaled air via mouth-based non-invasive biosensors for the detection of diabetes using nanotechnology-based approach.

ii. **Treatment (Drug delivery system)**

To formulate and characterize nanostructures:

a) Metallic nanoparticles

b) Lipidic nanoparticles

c) Polymeric nanoparticles

9. Work Timeline

Sr. no.	**Nature of work**	Duration of month
1.	Procuring of chemicals and reagent	3
2.	Preparation and characterization of sensing and nanostructure systems i. Biosensor ii. Metallic nanoparticles iii. Lipidic nanoparticles iv. Polymeric nanoparticles	12
3.	Comparative testing of nanoparticulate biosensor with conventional diagnostic method	1
4.	Development of method for *in-vitro* drug release studies	2
5.	Animal and stability studies	6
6.	Consolidation of reports for patents/ publication	3
7.	Thesis submission	3
	Total	**30**

Experimental work

1. **To determine the anti-diabetic activity of phthalocyanine in streptozotocin-induced rats**

The present study pioneered the anti-diabetic potential of phthalocyanine for hyperglycemia and hyperlipidemia in streptozotocin-induced diabetic rats.

Method

Male Sprague Dawley rats (180-220 g) were acquired from the National Institute of Biosciences, Pune for anti-diabetic study. The rats were quarantined for seven days under the conditions approved by the Committee for Control and Supervision of Experiments on Animals (CPCSEA), India in an animal house. The protocol was approved by the Institutional Animal Ethical Committee (IAEC) of the Shri Vile Parle Kelavani Mandal, Mumbai, India.

Experimental design

Animals were grouped into 4 containing ten rats in each. The groups were named Group I- Normal control group (CG), Group II- Negative diabetic group (NG), Group III- Diabetic group treated with 10 µg/kg of phthalocyanine (Pc1G) and Group IV- Diabetic group treated with 20 µg/kg of phthalocyanine (Pc2G). The experiment was carried out for 28 days with the daily dose administration via *i.v.* route.

Results

Bodyweight

The negative diabetic group showed decrease in body weight owing to the STZ induction without any treatment as represented in figure 1.

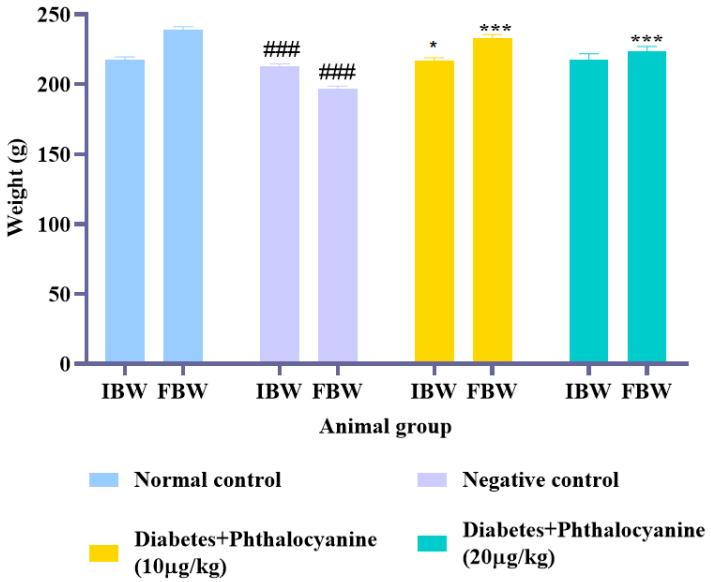

Figure 1. Initial body weight (IBW) and final body weight (FBW) of the diabetic rats. Each value expressed is mean ± SEM of 10 animals in each group. Statistical significance was calculated using two-way ANOVA (followed by the Dunnette comparison test) at *P= 0.0145 and ***P<0.0001 vs normal control group.

Blood glucose level

A significant rise in the glucose level was observed in comparison to the negative group during the experimental study may be due to the enhancement of glucose consumption by peripheral tissues mainly by muscle and adipose tissue.

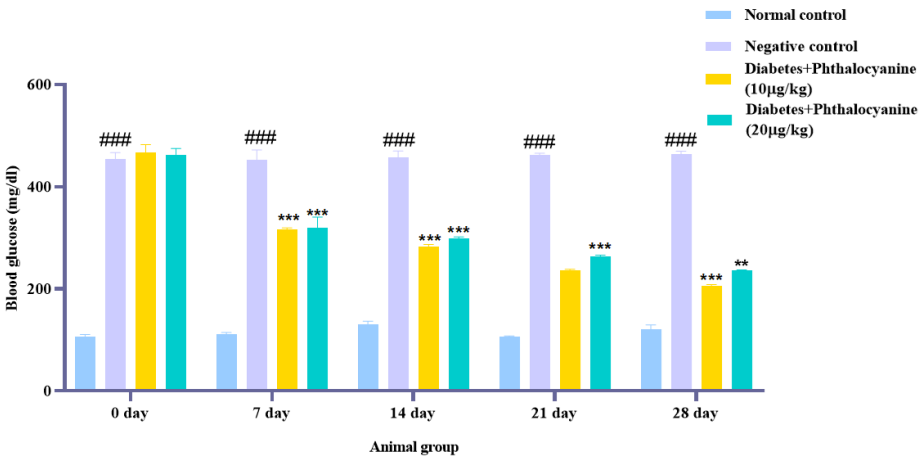

Figure 2. Blood glucose levels of different groups of animals. All values are expressed as Mean ± S.E.M, ***p<0.001 and **p<0.01 when compared with diabetic control group. ###p<0.001 when the diabetic control group compared with the normal control group.

Triglycerides, cholesterol, total protein content and alkaline phosphatase (ALP)

The triglyceride levels of animals treated with Pc at different doses like 10 µg/kg and 20 µg/kg was lowered in comparison to the negative diabetic group because of the effect of Pc to lower the levels of lipid peroxidation. STZ elevates the lipid level in the serum mainly by inhibiting the lipolytic hormone present on the fat depots responsible for hypertriglyceridemia.

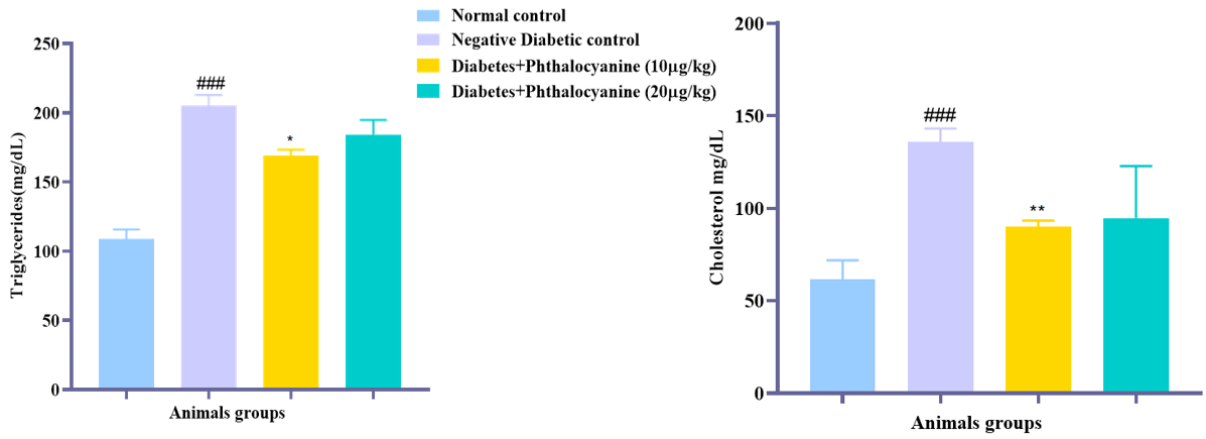

Figure 3. Serum triglycerides and cholesterol levels in STZ-induced diabetic rats at the end of the treatment period. All values are expressed as Mean ± S.E.M, ***p<0.001, **p<0.01 and *p<0.05 when compared with diabetic control group. ###p<0.001 when the diabetic control group compared with the normal control group.

Groups	Control group	Negative group	Pc1G	Pc2G
Total protein content (g/dL)	7.15±0.83	5.20±1.47	6.25±0.49	6.62±0.20

ALP (U/L)	12.47±2.58	21.49±4.38 (###)	14.82±1.78 (**)	14.11±4.21 (**)

Kidney Function Parameters

STZ increases the uptake by the proximal tubular cells and alters the tubular function with high urine protein excretion. This study proved that substantial enhancement in urine volume, total protein content and BUN levels in STZ-induced rats after 28 days, whereas there was a significant reduction in creatinine levels in STZ-induced rats.

Table 2. Effect of Pc on urine parameters

	Control group	**Negative group**	**PcLG group**	**PcNCA group**
TPC	30.45±7.01	180.23±4.71	142.23±2.71	120.43±5.04
BUN (mL/min)	1.51±0.36	0.61±0.21	0.89±0.73	1.01±0.67
Creatinine (mg/dl)	1.23±0.34	0.61±0.012	0.79±0.67	1.02±0.81

Figure 4. Effect of Pc on urine parameters. All values are expressed as Mean ± S.E.M, ***p<0.001, **p<0.01 and *p<0.05 when compared with diabetic the control group. ###p<0.001 when the diabetic control group compared with the normal control group.

Determination of oxidative stress parameters

Pc1G and Pc2G groups were able to reduce the catalase activity owing to the anti-oxidant activity of the Pc. In diabetic conditions, glutathione (GSH) oxidation decreases its synthesis, thus creating oxidative stress and weakening the cellular scavenging activity.

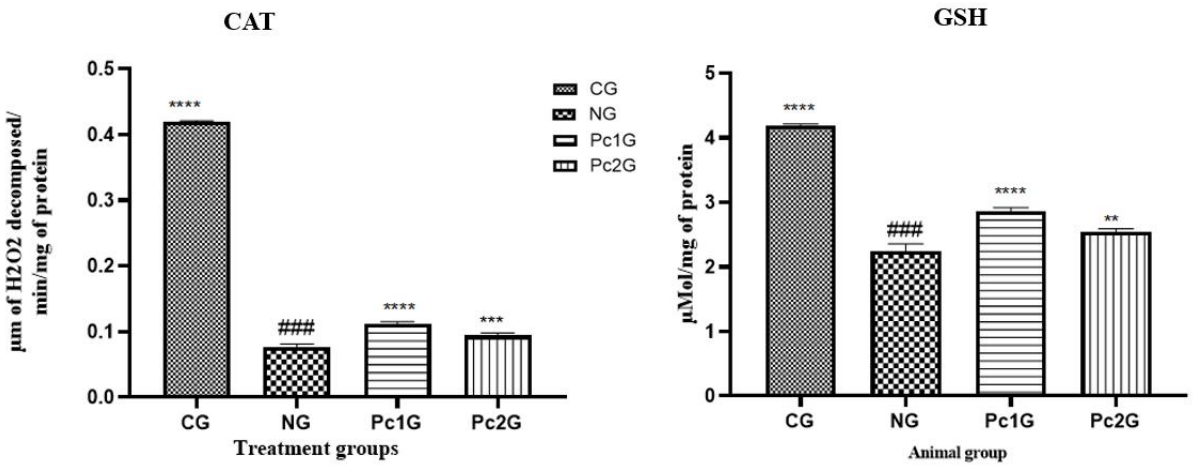

Figure 5. Effect of Pc on anti-oxidant parameters. CAT-catalase and GSH- Glutathione. All the values are expressed as Mean ± S.E.M, ***p<0.001, **p<0.01 and *p<0.05 when compared with the diabetic control group. ###p<0.001 when compared with the normal control group.

Histopathology of pancreatic tissue

The specimens of the diabetic group were affected by STZ as the lesions were formed in the distorted acini with ill-defined borders and significantly reduced thickness as shown in figure 6. The rats treated with 10 µg/kg and 20 µg/kg of Pc improved the pancreatic structure with basal rounded nuclei with well-defined boundaries of normal acini.

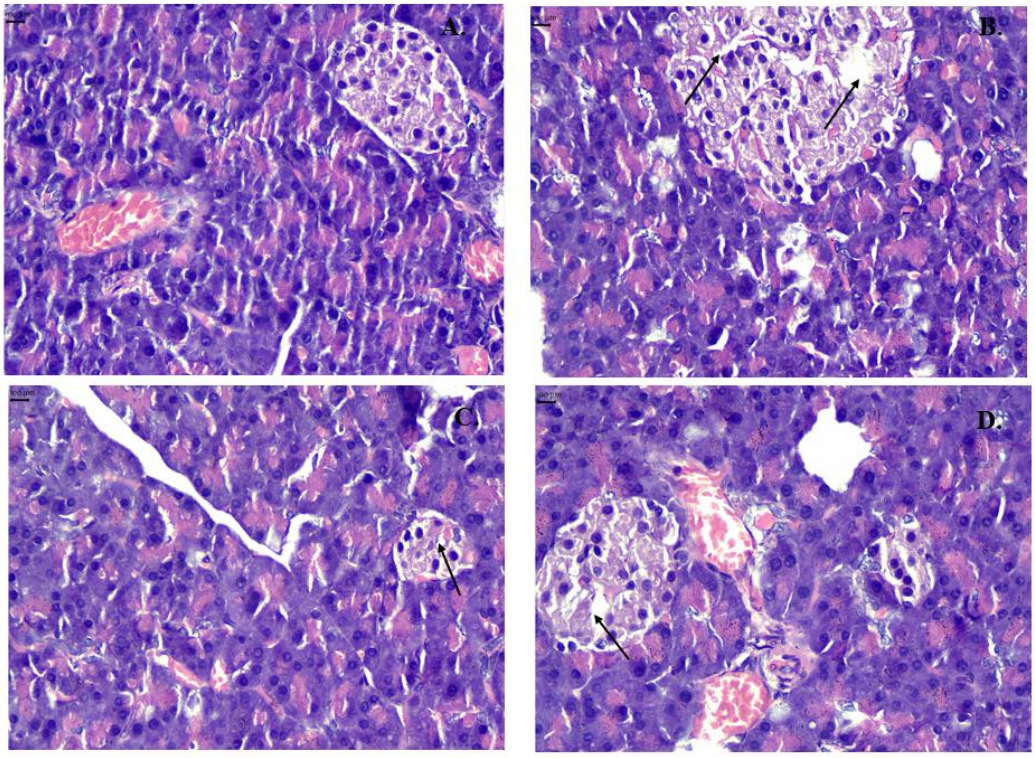

Figure 6. Effect of Pc on pancreatic tissue. A. Control group, B. Negative group, C. Diabetic group treated with 10 µg/kg of phthalocyanine and D. Diabetic group treated with 20 µg/kg of phthalocyanine

2. Preparation and characterization of phthalocyanine-loaded polymeric nanoparticles for streptozotocin-induced diabetic rats

The objective of the present diabetic research work was to fabricate and evaluate Pc-loaded nanosponges in the treatment of streptozotocin-induced diabetic animals by acting on the oxidative stress molecule and regenerating the pancreatic β-cell for the reduction in blood glucose level (<250 mg/dL).

Methods

Synthesis of phthalocyanine-loaded nanosponges (PNS)

Phthalocyanine-loaded nanosponges (PNS) were prepared using molar ratios of different concentrations of β-cyclodextrin and HMDI (1:4, 1:8, 1:10 and 1:12) by polymer condensation method.

Table 2. Formulation of blank nanosponges (BNS) and phthalocyanine-loaded nanosponges (PNS)

Sr. No.	Formulation	β-cyclodextrin: HMDI molar ratio		Phthalocyanine (g)
1.	BNS1	1	4	-
2	BNS2	1	8	-
3.	BNS3	1	10	-
4.	BNS4	1	12	-
5.	PNS1	1	4	0.5
6.	PNS2	1	8	0.5
7.	PNS3	1	10	0.5
8.	PNS4	1	12	0.5

Results

Particle size, zeta potential and PdI

The polymer condensation method was selected for the effective loading of Pc, due to its cost-effectiveness, moderate temperature reaction and ease of preparation at the laboratory scale

[25]. The PS, ZP and PdI of the Pc, formulations BNS1, BNS2, BNS3, BNS4, PNS1, PNS2, PNS3 and PNS4 were determined using dynamic light scattering and results are stated in Table 3.

Table 3. Physicochemical characteristics of BNS and PNS (Mean ± SD, n=3)

Sr. No.	Formulation	Particle size (nm±SD)	PdI (n±SD)	Surface charge (mV±SD)
1.	Pc	2059.12±9.26	1.000±2.06	-31.59±0.56
2.	BNS1	421.89±2.45	1.000±1.17	-21.59±1.52
3.	BNS2	281.59±0.78	0.259±2.12	-29.89±0.23
4.	BNS3	389.05±2.70	0.321±0.99	-11.18±0.75
5.	BNS4	269.8±0.59	0.408±1.04	-25.06±0.26
6.	PNS1	421.89±1.76	1.000±1.23	-24.59±1.52
7.	PNS2	328.12±1.02	0.359±2.87	-35.08±0.89
8.	PNS3	389.05±2.7	0.359±1.45	-19.18±0.75
9.	PNS4	354.35±0.89	0.402±2.23	-31.14±1.59

% Entrapment efficiency

The entrapment of the drug in nanosponges were manipulated by varying the degree of HMDI to form a flexible network.

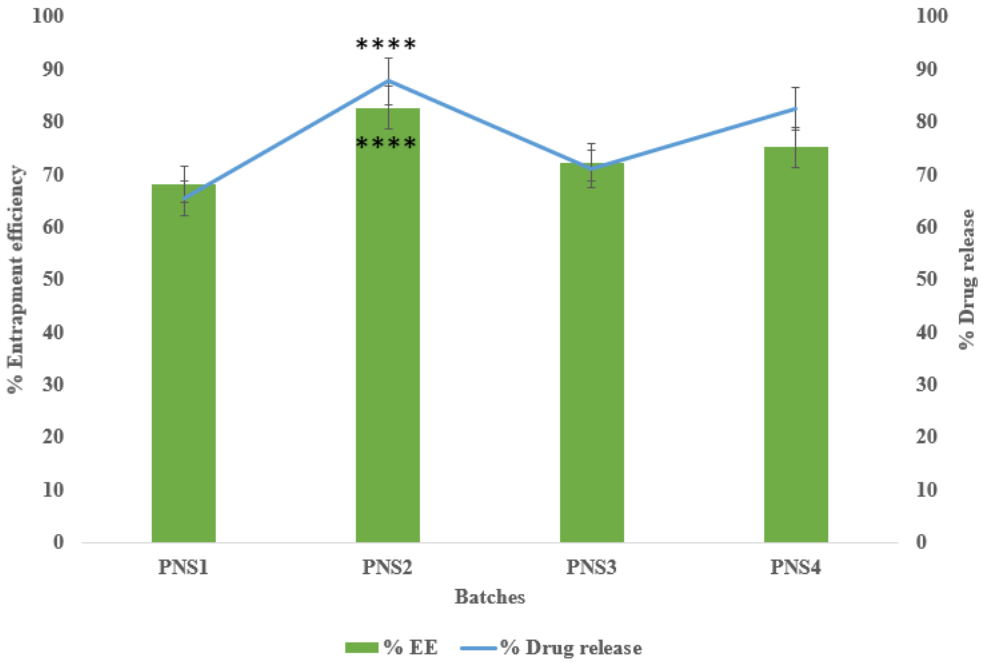

Figure 7. Entrapment efficiency and *in-vitro* drug release studies of formulation PNS1, PNS2, PNS3 and PNS4. All the values are expressed as Mean ± S.D.**p<0.0001 when compared with Pc.**

***In-vitro* drug release studies**

Formulations PNS1, PNS2, PNS3 and PNS4 demonstrated 65.45±1.56%, 87.8±2.09%, 71.17±0.49% and 82.5±1.96% release, respectively in release medium for the period of 36 h (P<0.0001).

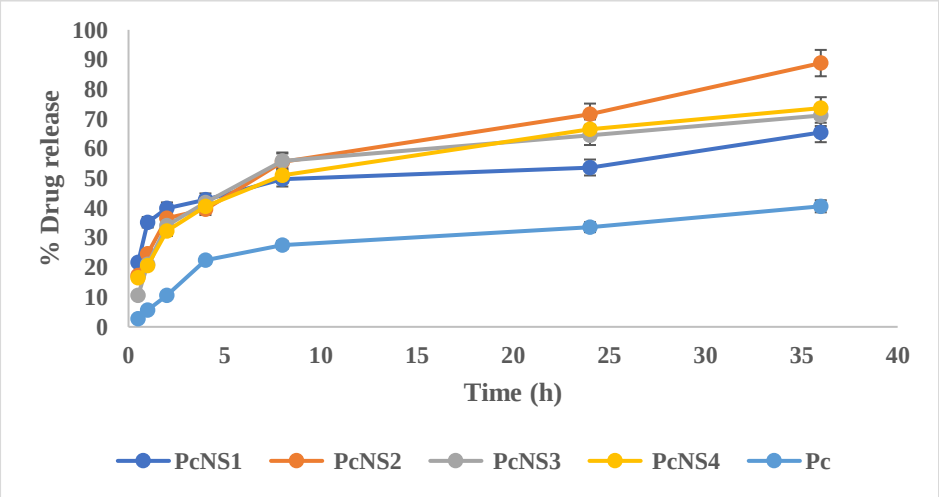

Figure 8. % Drug release profiles of formulations PNS1, PNS2, PNS3 and PNS4

Considering the particle size, surface charge, PdI value, % EE and *in vitro* release studies, formulation PNS2 was selected further for surface morphology, DSC, FTIR, XRPD, NMR, anti-oxidant and animal studies.

Surface morphology

Figure 9. shows the SEM images of Pc and formulations BNS2 and PNS2. The surface morphology of Pc (Figure 4A) showed the crystalline nature with a smooth surface whereas formulation BNS2 (Figure 4B) displayed the rough, porous and slightly irregular surface of the nanosponges with the size range of 100-300 nm and better size distribution.

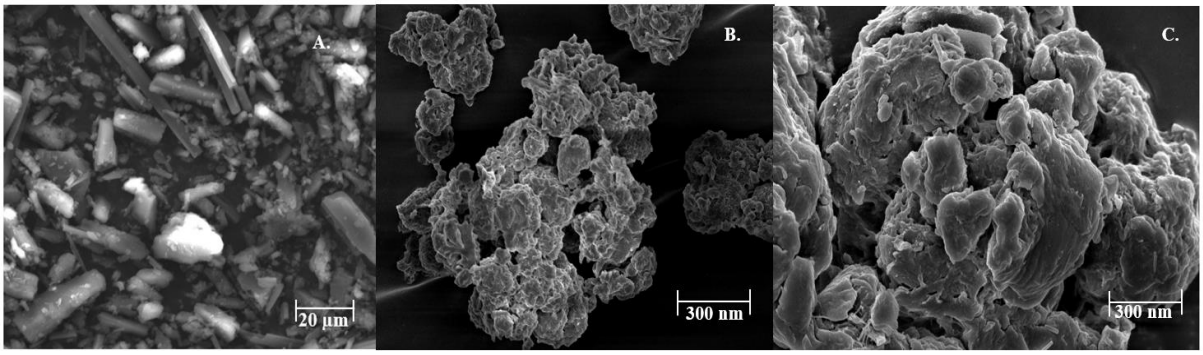

Figure 9. SEM images of A. Pc, B. Formulation BNS2 and C. Formulation PNS2

Fourier transform infrared spectroscopy (FTIR)

The FTIR spectra of β-cyclodextrin, Pc, formulations BNS2 and PNS2 are mentioned in Figure 10. The FTIR spectrum of β-CD in Figure 3A displays the C-H stretch vibration at 1412 and 1334 cm-1, O-H stretch at 3299 cm-1, and -H distortion vibrations and glucopyranose stretch at 939, 852, and 754 cm-1.

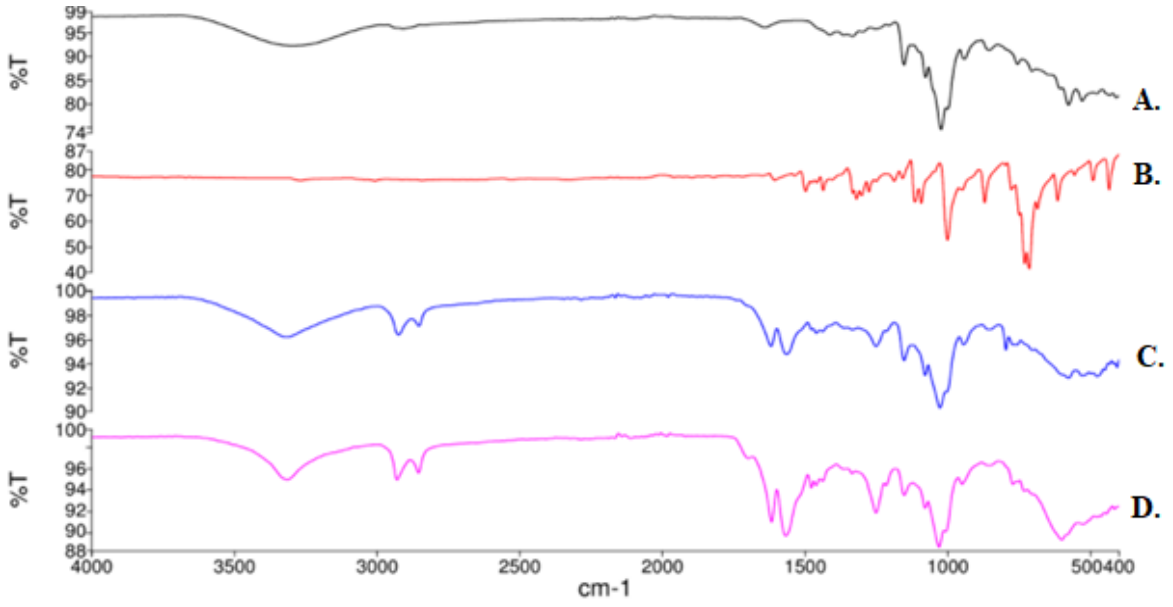

Figure 10. FTIR spectra of A. β-cyclodextrin, B. Pc, C. Formulation BNS2 and D. Formulation PNS2

Thermal analyses

The DSC curves of Pc, formulations BNS2 and PNS2 determined the interaction between dye and β-CD. The thermograph of Pc displayed a typical endothermic peak at 240−280 °C corresponding to its melting point as shown in Figure 11.

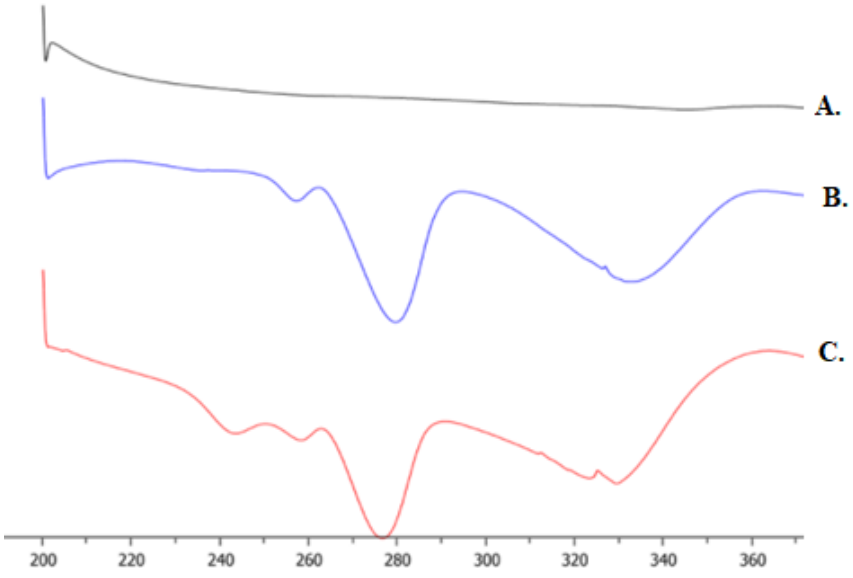

Figure 11. DSC thermograms for A. Pc, B. Formulation BNS2 and C. Formulation PNS2

X-Ray Powder Diffraction (XRPD)

The comparison of XRPD diffractograms of Pc, formulations BNS2 and PNS2 displayed significant changes in the characteristic peaks as shown in Figure 12. The peaks of Pc at diffraction angles 2 Theta (2θ) of 6.716, 8.912, 14.83, 17.91, 27.72 and 30.04 were entirely weakened in the formulation PNS2, owing to the development of new amorphous solid structure.

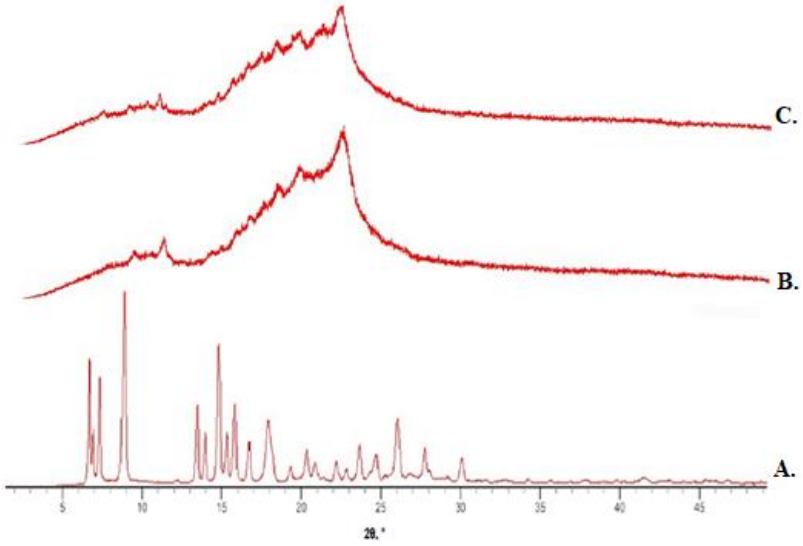

Figure 12. XRPD pattern of A. Pc, B. Formulation BNS2 and C. Formulation PNS2

DPPH radical scavenging assay

The anti-oxidant potentials of Pc and formulation PNS2 were examined using DPPH free radical assay. DPPH is considered a steady molecule that is mainly depleted by accepting hydrogen or electrons. The study parameters include the scavenging activity at different concentrations ranging from 25-100 µg/mL.

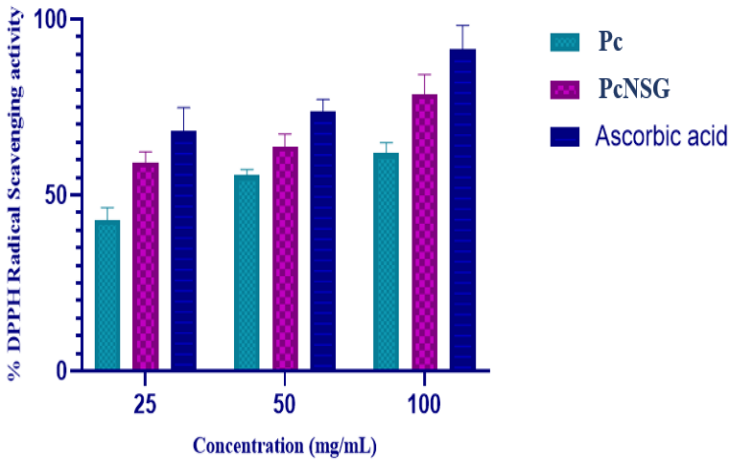

Figure 13. The rate of DPPH scavenging in presence of Pc, formulation PNS2 and ascorbic acid as a standard. All the values are expressed as Mean ± S.E.M,**p<0.0001 and ***p<0.001 when compared with formulation BNS.**

Animal studies

Body weight

Body weight was recorded of all treatment groups on day 0 and later the completion of the experimental period on 28th day as shown in Figure 14. The negative group (Diabetic group) of rats exhibited a notable decrease in the body weight (P<0.0001) in comparison with the initial body weight.

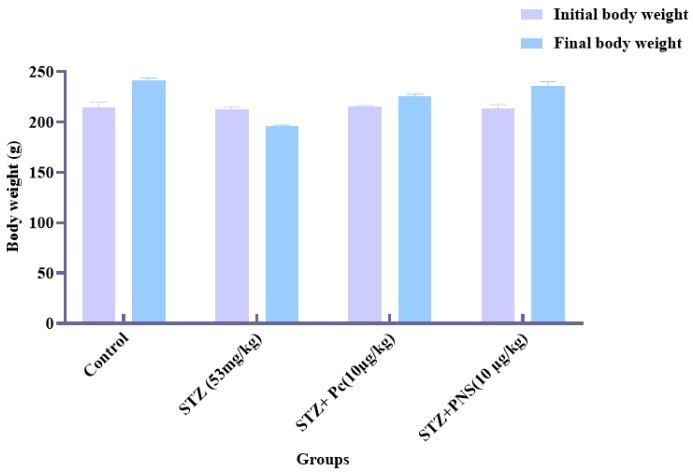

Figure 14. Effect of Pc and formulation PNS2 treatment on body weight in rats

Blood glucose estimation

The glucose level was checked for rats at different time intervals (0 day, 7th day, 14th day, 21st day and 28th day) as shown in Figure 15. The administration of STZ progressively damaged the pancreatic tissues, thus displayed higher levels of blood glucose levels (P<0.0001) as compared to control group.

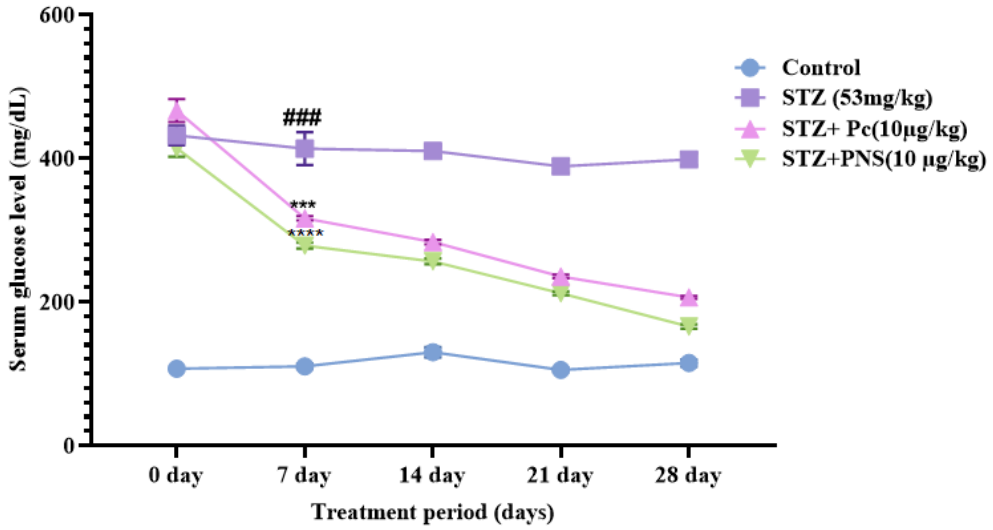

Figure 15. The blood glucose levels in different groups of animals during the 4-week experiment. All the values are expressed as Mean ± S.E.M,**p<0.0001 and ***p<0.001 when compared with diabetic control group. ###p<0.001 when compared with control group.**

Biochemical assays

Hypercholesterolemia is related to distressed angiogenesis, which delayed the tissue healing progression. The alleviation in the lipids due to STZ involve the healing of tissues of rats treated with formulation PNS. Increased transaminase levels owing to the extreme leakage of these

enzymes into the bloodstream, is one of the indicators for hepatic dysfunction caused by the STZ induction.

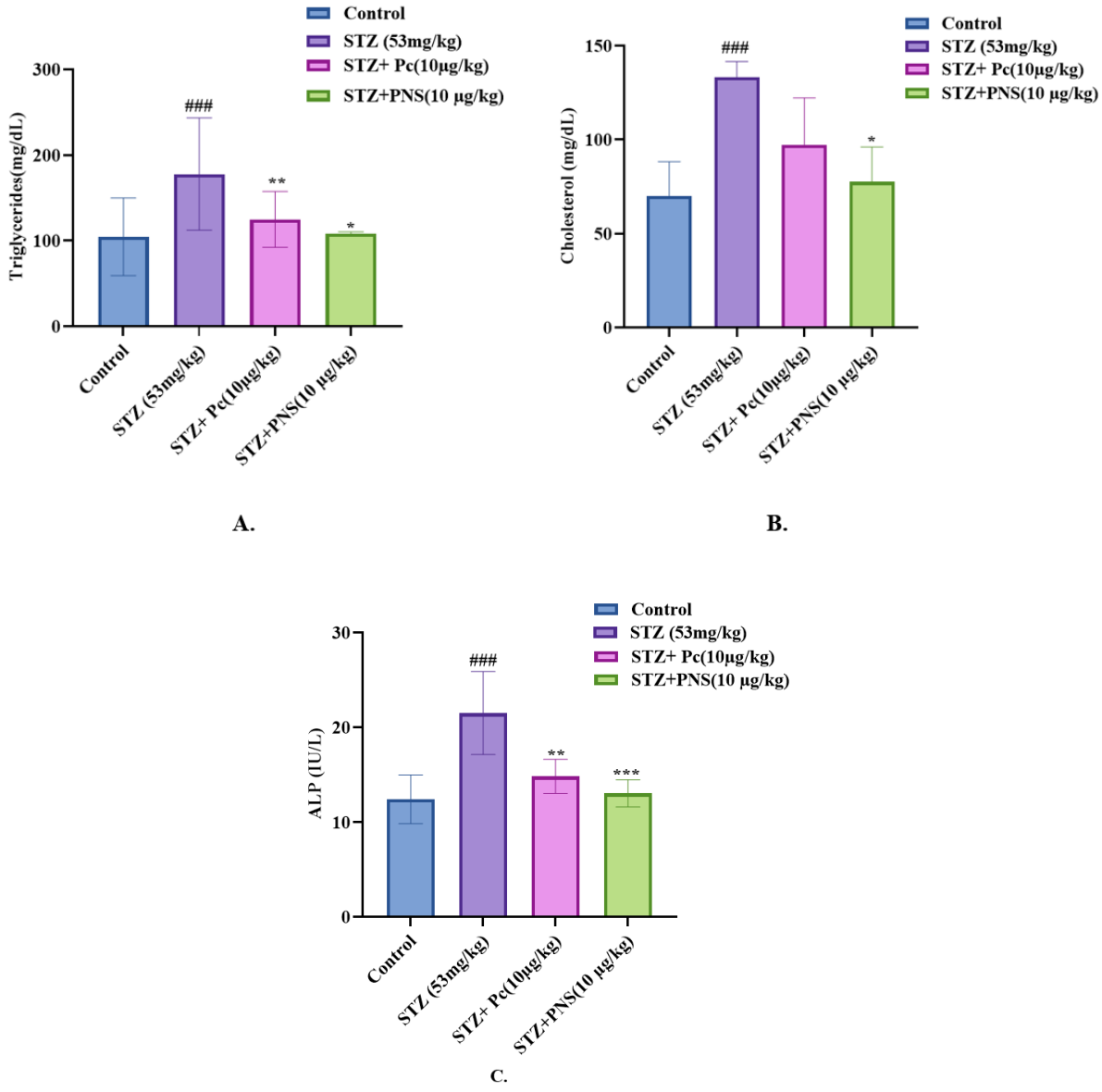

Figure 16. Effect of Pc and formulation PNS2 on serum: A. triglyceride, B. cholesterol and C. ALP levels in diabetic rats. All the values are expressed as Mean ± S.E.M,**p<0.0001, ***p<0.001, **p<0.01 and *p<0.05 when compared with diabetic control group. ###p<0.001 when compared with control group.**

Estimation of total protein content (TPC)

Table 4. represents the significant increase in serum total protein content for the formulation PNS2 treated group as compared to diabetic group.

Table 4. Total protein content in serum of diabetic groups

Groups	Control	STZ (53mg/kg)	STZ+ Pc(10µg/kg)	STZ+PNS(10 µg/kg)
Total protein content (g/dL)	7.15±4.31	5.21±3.92	6.25±4.01	6.75±5.31

Parameters evaluated from urine

During the experimental period, it was observed that the STZ-treated group exhibited higher protein excretion altering the capillary filtration barrier which resulted to enhance penetrability of the glomerular basement membrane. (Figure 17).

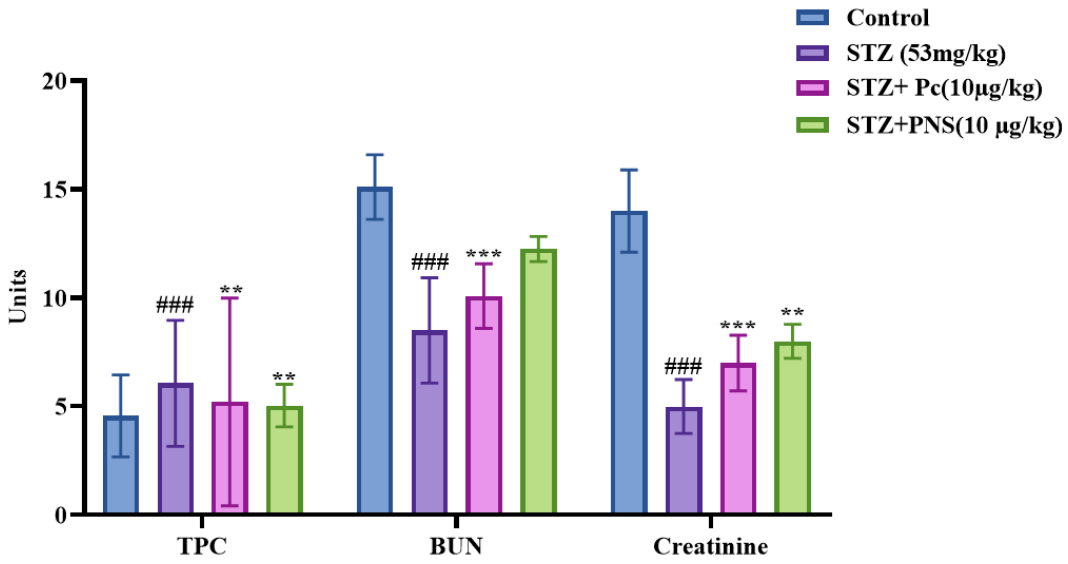

Figure 17. Effect of Pc and formulation PNS2 on urine: A.Total protein content, B. BUN and C. Creatinine in diabetic rats' urine. All the values are expressed as Mean ±

S.E.M,**p<0.0001, ***p<0.001 and ** p<0.01 when compared with diabetic control group. ###p<0.001 when compared with control group.**

Determination of oxidative stress parameters

Catalase activity was significantly reduced in the STZ-induced rats in comparison to the control group, owing to the anti-oxidant ability of the Pc. GSH, is another antioxidant agent involved in nutrient breakdown, antioxidant defense and regulation of cellular metabolic functions. It scavenges the unstable atoms directly as well as substratum the peroxide detoxication as shown in figure 18.

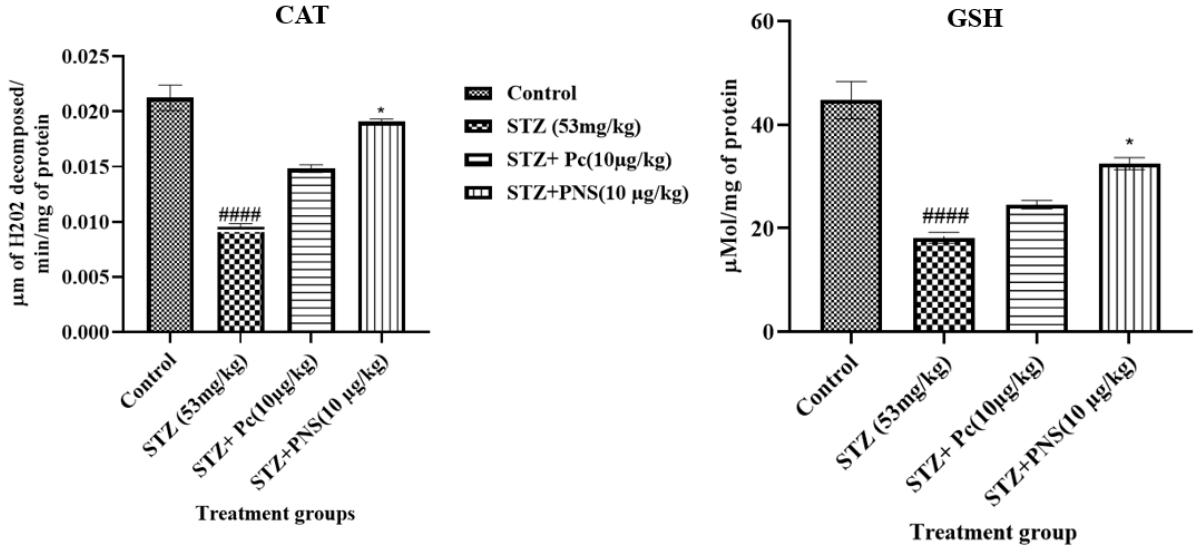

Figure 18. Effect of Pc and formulation PNS2 on antioxidant status of liver in diabetic rat. All the values are expressed as Mean ± S.E.M, *p<0.05 when compared with diabetic control group. ###p<0.001 when compared with control group.

Histopathology of pancreatic tissue

The histopathologic analysis of pancreatic tissue displayed acute blockage, an observable reduction in the number of islets of Langerhans, β-cells and inflammatory tissue aggression in STZ-induced diabetic group. Meanwhile, the group treated with formulation PNS2 for 4-weeks

proved significant development in the decellularization of the islets of Langerhans and peripheral islet infiltration of lymphocytes when associated with Pc-treated group as shown in Figure 19.

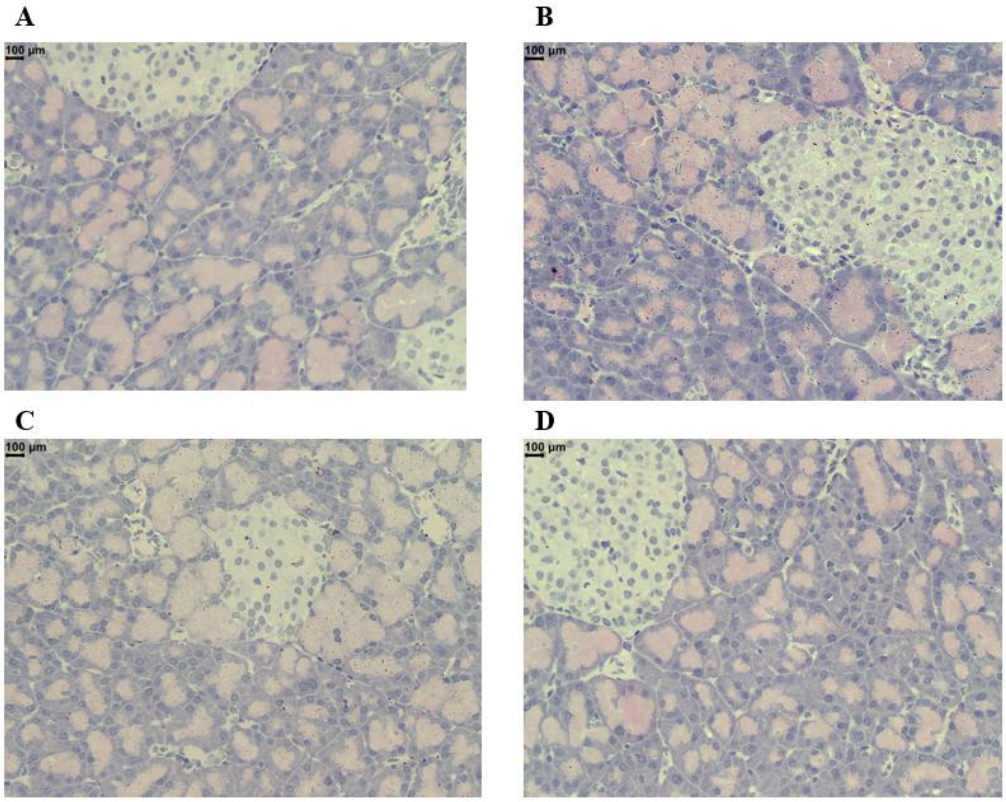

Figure 19. Histopathology examination of pancreas sections: A. control group (CG), B. negative group, C. diabetic animals with Pc and D. diabetic animals with formulation PNS2

3. Preparation and characetrization of concanavalin A-conjugated phthalocyanine cochleates for STZ-induced diabetic rats

The present research work aimed to fabricate and characterize Con A conjugated phthalocyanine-loaded cochleates to mitigate the hyperglycaemic, hyperlipidaemic and oxidative damage in streptozotocin (STZ)-induced diabetic rats.

Fabrication of Pc-loaded liposomes using thin-film hydration method (PhLPs)

Pc was encapsulated with thin-film hydration method in liposomes by using lipids like dipalmitoylphosphatidylcholine, Lipova L-120®, stearylamine and cholesterol dissolved in ethanol (5mL). Briefly, a specific amount of Pc (10 mg), DPPC, LL-120, cholesterol and stearyl amine in different ratios were added to the minimum quantity of ethanol as shown in Table 5. Rota-evaporator (RV 10 auto pro-V, China) was used to evaporate the organic phase under reduced pressure at 55^{o}C with 100 rpm until the thin film of lipid Pc mixture was formed on the inside wall of the flask. Later, the lipoidal film was hydrated with 8 mL of buffer (pH 7.4) with the flask revolving at 37^{o}C in a water bath for 30 min.

Table 5. Composition of different formulations for PhLPs

Formulation	Lipid		Cholesterol (mg)	Stearylamine (mg)	Drug (mg)
	DPPC (mg)	LL-120 (mg)			
PhL1	100	-	100	50	10
PhL2	-	100	100	50	10
PhL3	75	25	100	50	10
PhL4	25	75	100	50	10
PhL5	50	50	100	50	10
PhL6	75	25	50	50	10
PhL7	25	75	50	50	10
PhL8	50	50	50	50	10

Based on the particle size, zeta potential, PdI values and % encapsulation efficiencies, PhL6 was considered further for cochleates preparation.

Preparation of Pc-loaded nanocochleates (PhNCs) using trapping film method

Pc-loaded nanocochleates (PhNCs) were prepared using the trapping method (figure 20) with 20 µL of $CaCl_2$ (10 mM) added to 10 mL of formulation PhL6 and stirred at 650 rpm at 37°C. The turbid phase appearance indicated the formation of PhNCs which were then stored in cool conditions to enhance the yield. The above sample was centrifugated at 15000 rpm for 10 min at 4°C and used further for Con A conjugation.

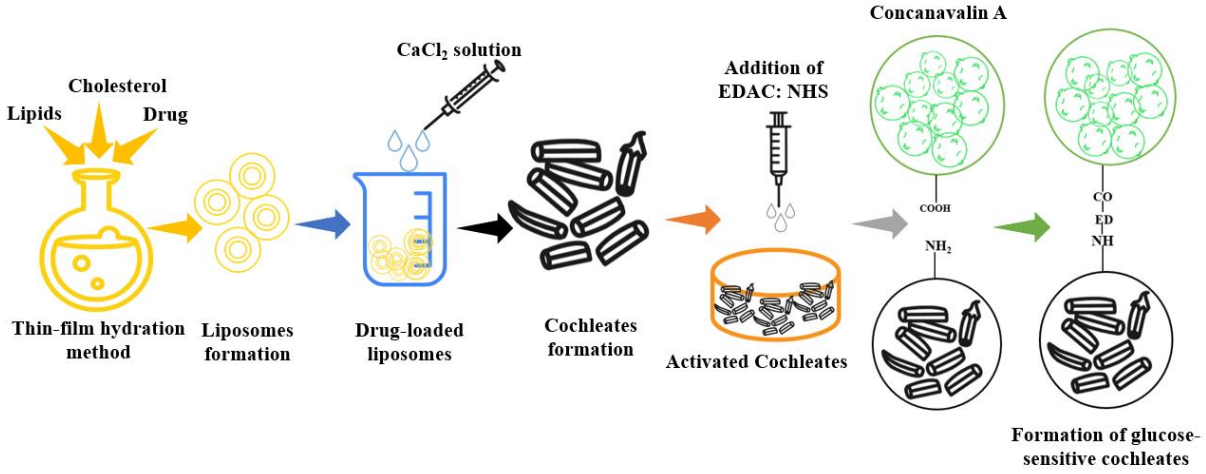

Figure 20. Preparation of glucose-sensitive cochleates

Preparation of Con A-conjugated PhNCs (PhConA)

Con A was conjugated to formulation PhNCs using the procedure (figure 1) designated by Hurkat et al. (2012) with slight modification (Hurkat *et al.* 2012a). The centrifuged PhNCs (1 mL) were activated using 1 mL of 0.7 M N-hydroxysuccinimide (NHS) and 0.1 M 1-ethyl-3-(3-dimethylaminopropyl) carbodiimide (EDAC) to conjugate the amine group of Con A with the carboxylic groups of PhNCs and mixed at ambient conditions for 60 min.

Results and discussion

Pc-loaded liposomes

The order of particle size for the Pc-loaded liposomes was found to be PhL6 (320.67± 5.97) > PhL3 (345.54± 1.58) > PhL2 (397± 2.18) > PhL8 (648.7± 0.89)> PhL7 (725.8± 3.56) > PhL4 (830.7± 3.56) > PhL5 (894. ± 1.65) > PhL1 (1119± 32.64). The ZPs of Pc-liposomes were also observed in the range of -1 to -25 mV directed the stability of the nanosystem in the bloodstream, as ZP is considered a vital parameter for *intravenous* administration.

Table 6. Summarized results of physicochemical characterization

Formulations	***PS (nm±S.D.)***	***PdI (n±S.D.)***	***ZP (mV±S.D.)***	***% EE (%±S.D.)***
PhL1	1119.81± 32.64	1.00± 0.65	-1.9± 2.56	54.45±2.34
PhL2	397.49± 2.18	1.00± 1.09	-0.594±0.34	64.34±0.12
PhL3	345.54± 1.58	0.45± 4.23	-25.65± 3.12	69.56± 3.09
PhL4	830.7± 3.56	0.58± 2.56	-15.67±1.65	59.43± 4.56
PhL5	894.65 ± 1.65	0.35± 0.89	-11.23±3.09	45.83± 0.09
PhL6	**320.67± 5.97**	**0.36± 1.45**	**-21.8±0.04**	**82.43±4.34**
PhL7	725.89± 3.56	0.16± 3.67	-13.56±3.43	74.65±2.76
PhL8	648.71± 0.89	0.53± 2.78	-24.67±3.01	75.43±1.23

Pc-loaded cochleate (Formulation PhNCs)

Formulation PhL6 with least PS and high encapsulation efficiency was optimized for cochleate preparation (Formulation PhNCs). Adding calcium ions to the liposomes fuses the lipidic

membrane for the formation of planar sheets and further coiled the initial lipidic membrane for the formation of rod-shaped cochleates.

Concanavalin A conjugated Pc-loaded cochleate (Formulation PhConA)

The average PS, ZP and PdI value of formulation PhConA were found to be 415.7 ± 0.46 nm, -10.23± 0.46 mV and 0.435, respectively. Conjugation of bulky molecules like concanavalin

% Entrapment efficiency

The combinational effect of DPPC with Lipova L-120 facilitated greater encapsulation efficiency as compared to the single lipid effect. The comparison between the formulations PhL6, PhL7 and PhL8 showed that the ratio DPPC: Lipova L-120 (75:25) improved the EE upto 82.43±4.34%.

% Encochleation efficiency

For the formulation PhNCs, the encochleation efficiency was 85.64±0.34 % better than liposomes because of the encapsulation of the free drug.

Transmission Electron Microscopy (TEM)

TEM study was performed to confirm the surface morphology and particle size distribution of Pc-loaded liposomes, formulations PhNCs and PhConA. Pc-loaded liposomes exhibited uniform homogeneous spheroidal structure with sizes upto 100 nm.

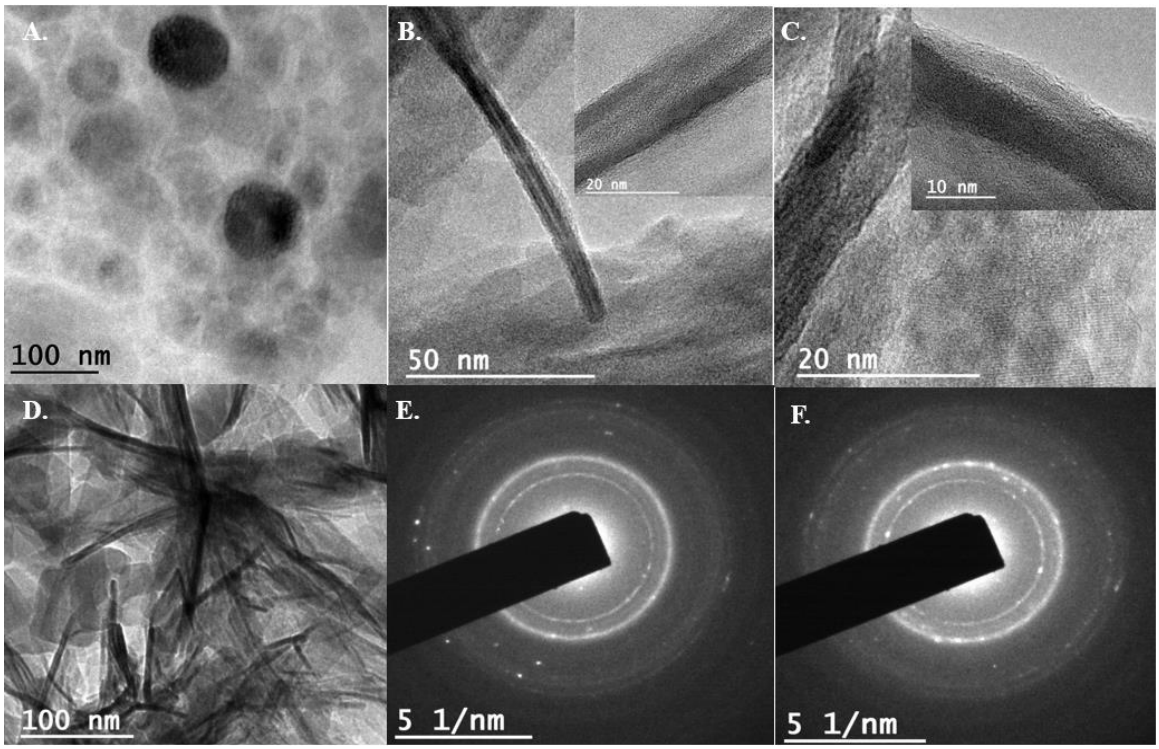

Figure 20. Transmission electron microscope images of A. Pc-loaded liposomes, B. Blank-cochleate, C. Formulation PhNCs, D. Formulation PhConA, E. Diffraction pattern of formulation PhNCs and F. Diffraction pattern of formulation PhConA.

FTIR

FTIR spectra of Pc, Lipova L-120, DPPC, cholesterol, concanavalin A, formulation PhNCs and formulation PhConA are mentioned in Figure 21. Peaks of Pc were observed at 1329 and 1380 cm^{-1} accredited to pyrrole stretch and the symmetric C-H bend at -CH3 groups in acetyloxy side chains with the frequency from 1312–1318 cm^{-1}.

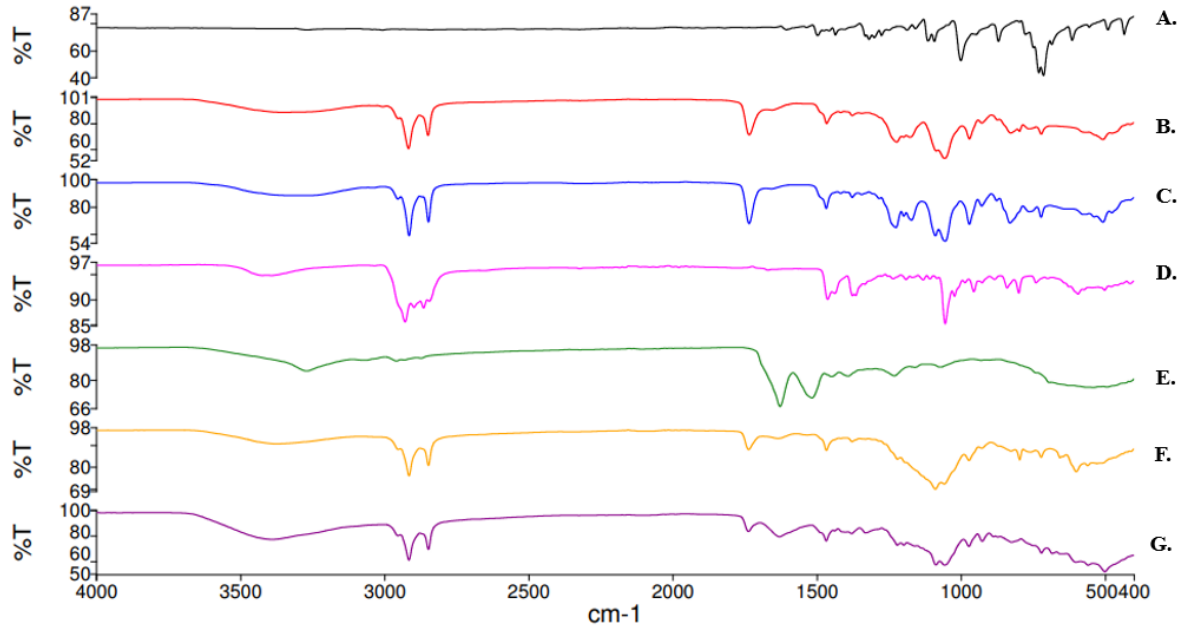

Figure 21. FTIR spectra of A. Pc, B. DPPC, C. Lipova L-120, D. Cholesterol, E. concanavalin A, E. Formulation PhNCs and F. Formulation PhConA

Thermal analysis

DSC was executed to determine the thermal behaviour of Pc in Pc-loaded liposomes, formulations PhNCs and PhConA (Figure 22). The Pc in figure 4c endothermic peak at 280°C is about its melting point to specify the crystalline nature of drug.

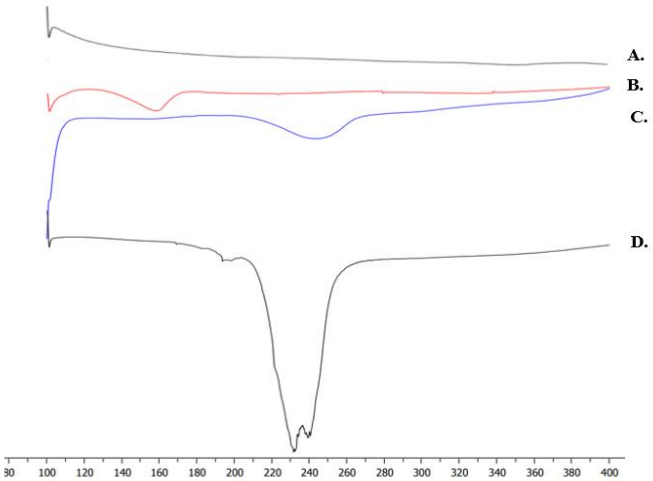

Figure 22. Thermal analyses of A. Pc, B. Pc-loaded liposomes, C. Formulation PhNCs and D. Formulation PhConA

X-ray diffraction study (XRD)

XRD patterns of Pc, Pc-loaded liposomes and formulation PhConA are shown in figure 23. Pc and formulation PhConA displayed the crystalline physical nature of formulation, while Pc-loaded liposomes emphasized the para-crystalline nature of lipids.

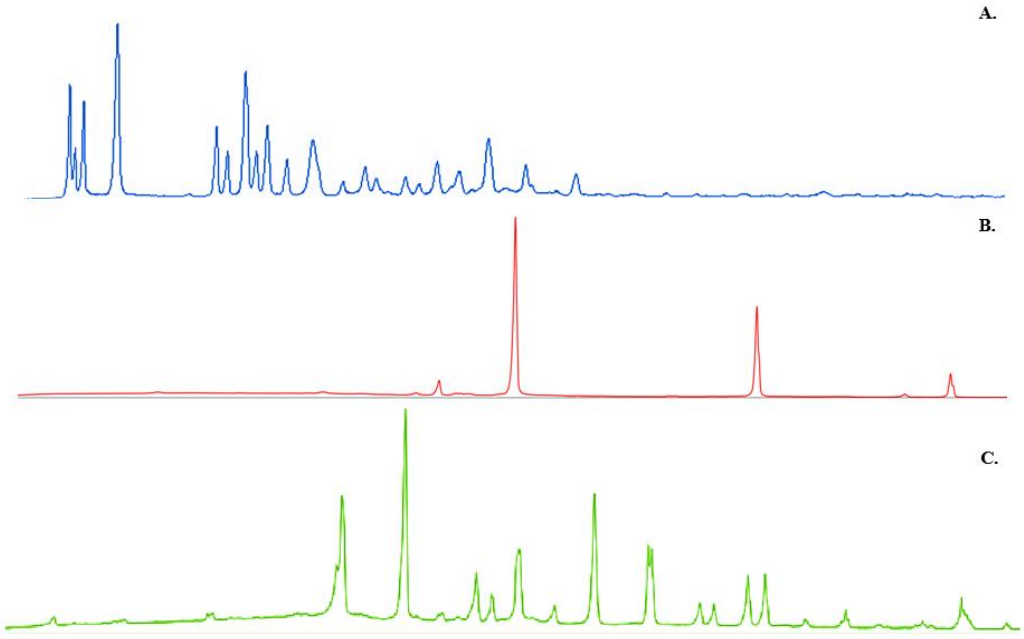

Figure 23. Powder X-ray diffraction of (A)Pc, (B) Pc-loaded liposomes and (C) Formulation PhConA

Circular dichroism study (CD spectrum)

Figure 24 denotes the structural integrity of concanavalin A after the encapsulation into PhConA. Prevention of structural integrity is important for protein after the formulation enters the biological system. The CD spectrum of concanavalin A proved negligible change in Con A after the conjugation with formulation PhNCs.

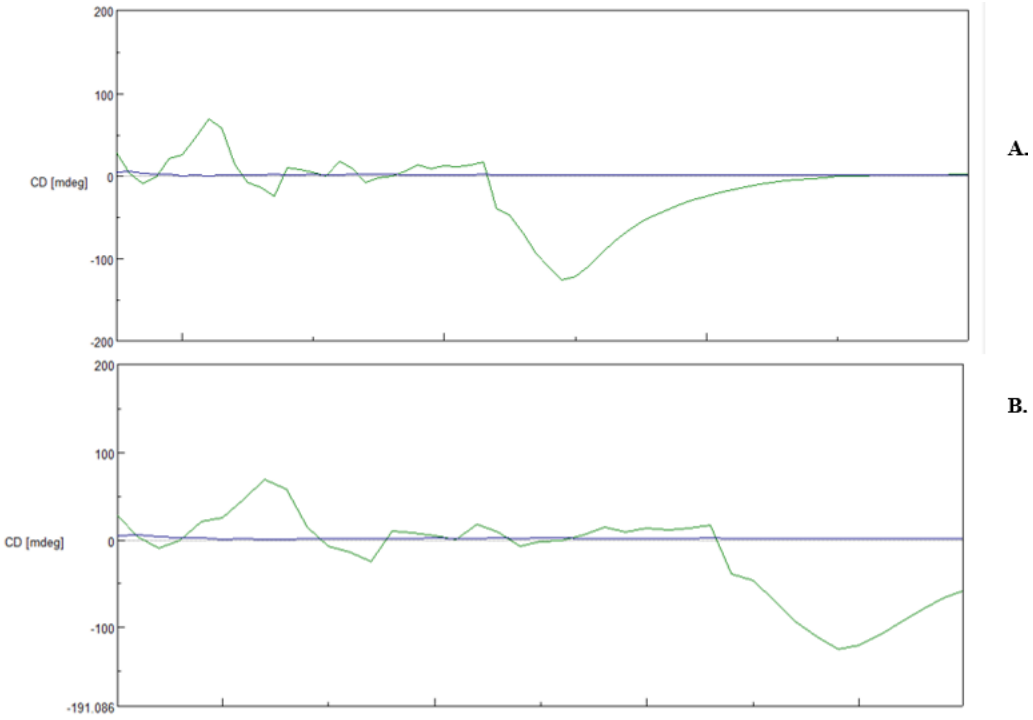

Figure 24. CD-spectra of A. Concanavalin A and Formulation PhConA

***In vitro* enzymatic degradation study**

Figure 25 shows the lipid loss of the particles under the presence of lysozymes dispersed in PBS pH 7.4. It was observed that the particles showed higher degradation under the presence of lysozymes within the period of 48 h. LL-120 is a natural phospholipid that might have led to slow degradation of the cochleates.

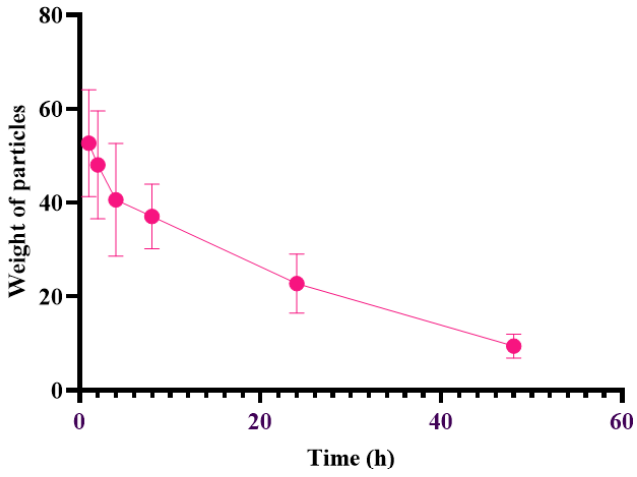

Figure 25. Biodegradation pattern of cochleates under the influence of lysozymes in phosphate buffer pH 7.4.

% Drug release studies

Release studies of Pc from formulations PhL6 and PhNCs were observed in PBS pH 7.4 using dialysis membrane method at 37°C. The release patterns of Pc and formulation PhL6 and PhNCs were observed to be 47.89±2.89%, 72.09±1.09% and 84.55±0.29 %, respectively for the period of 48 h as shown in figure 9. Formulations of PhL6 and PhNCs showed 40% release of Pc within the period of 4 h followed by the controlled release upto 72.09±1.09% and 84.55±0.29% for 48 h.

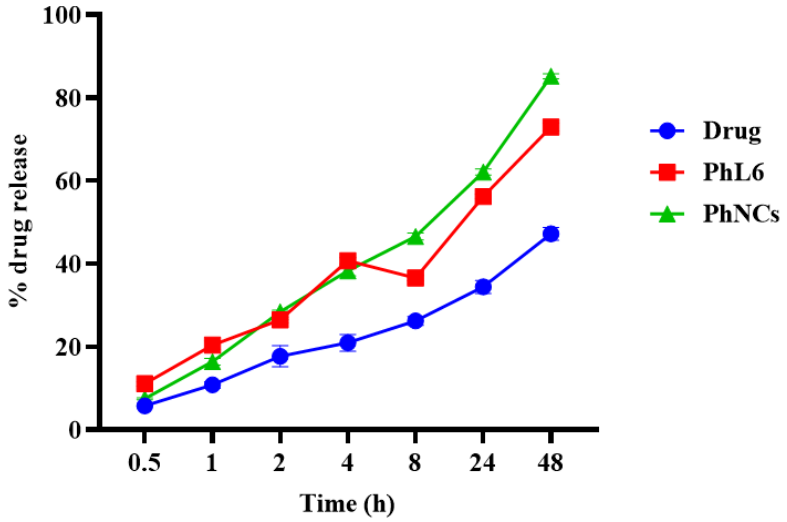

Figure 26. *In vitro* release profile of Pc plain, formulations PhL6 and PhNCs in phosphate buffer saline pH 7.4

Animal studies

Bodyweight

Diabetic rats displayed a weight loss in comparison to the normal group ($p<0.001$) during the 28 days of study shown in Figure 27. However, the groups treated with Pc and formulation

PhNCs displayed significant weight gain in comparison to negative diabetic group ($p<0.05$ and $p<0.001$).

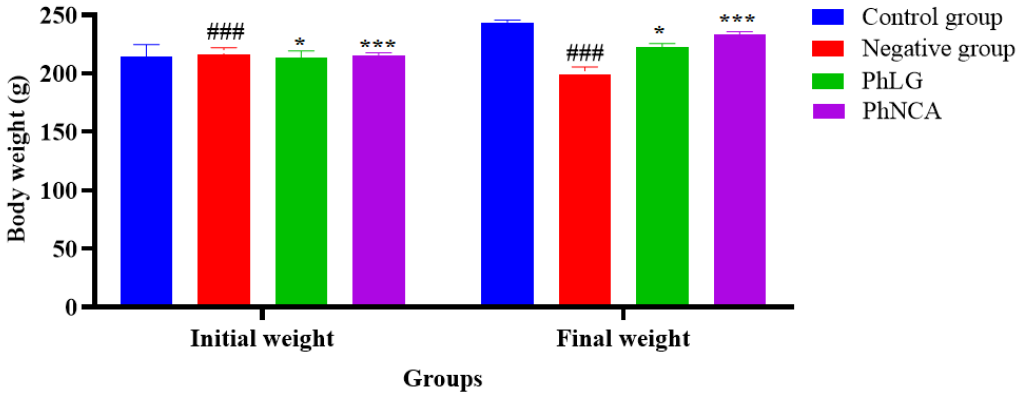

Figure 27. Effect of Pc and formulation PhConA on body weight. All values are stated as Mean ± S.E.M, ***p<0.001 and *p<0.05 in comparison to diabetic control group. ###p<0.001 when compared with the normal control group

Biochemical parameters investigation

Blood glucose level

Figure 28 represents the consequence of phthalocyanine and formulation PhConA on blood glucose levels within 28 days. After the diabetes induction, the pre-treatment blood glucose level was found to be >250 mg/dl, suggestively more than the normal group ($p < 0.05$) indicated the diabetic induction in rats. The blood glucose level significantly reduced in the animals with Pc ($p <0.0001$) along with the formulation PhConA ($p <0.0001$) in comparison to the control group ($p < 0.05$).

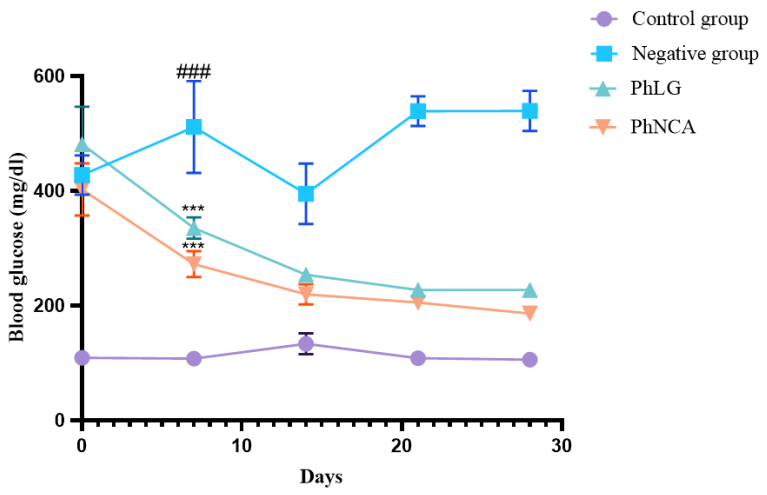

Figure 28. Effect of Pc and formulation PhConA on blood glucose levels in diabetic rats. All the results expressed are Mean ± S.E.M, ***p<0.001 and *p<0.05 in comparison to diabetic control group. ###p<0.001 compared to control group.

Lipid parameters, total protein content and ALP

The serum cholesterol and triglycerides concentrations in diabetic rats are mentioned in Figures 29 A. and B. As compared to the normal group, the diabetic group showed higher cholesterol (>180 mg/dl) and triglycerides levels (>230 mg/dl) p<0.05) due to the increase in intestinal acyl-coenzyme A: cholesterol acyltransferase (ACAT) caused by STZ.

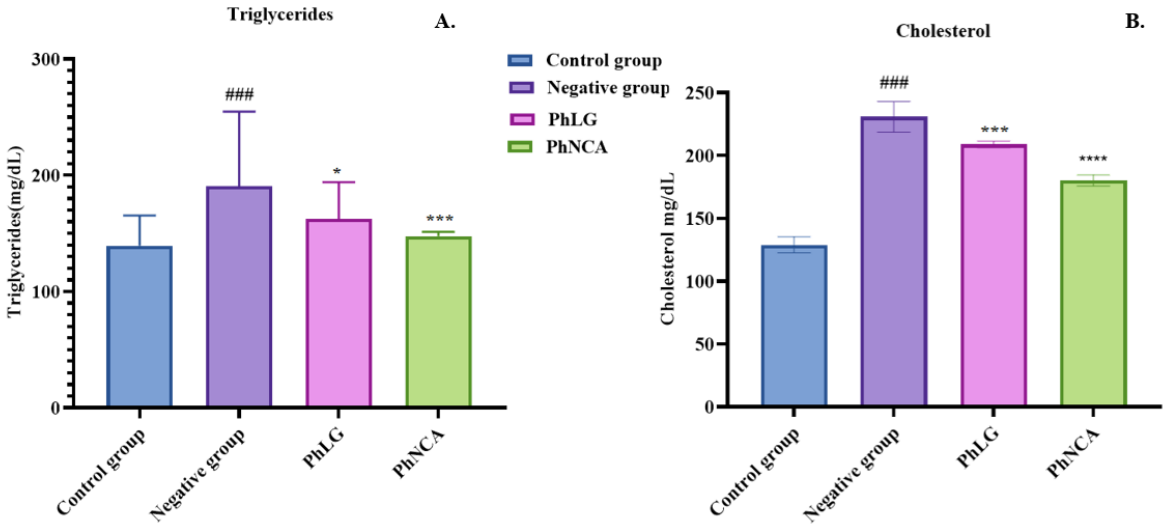

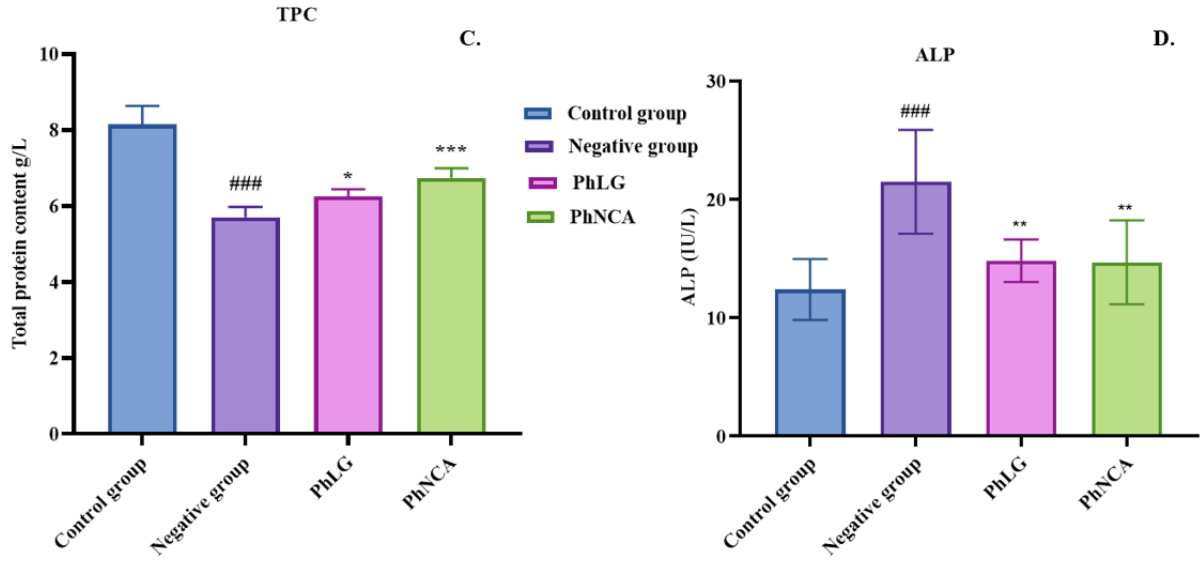

Figure 31. Effect of Pc and formulation PcConA on A. Triglycerides and B. Cholesterol. All the values expressed are Mean ± S.E.M, ***p<0.001 and *p<0.05 in comparison with diabetic control group. ###p<0.001 when the diabetic control group compared with the normal control group

Urine parameters

The nitrogen synthesis imbalanced by generating STZ non-protein nitrogenous components such as creatinine and blood nitrogen urea. Kidney abnormalities alter renal hemodynamic glomerulosclerosis, renal dysfunction and proteinuria.

Table 8. Levels of total protein content, BUN and creatinine level in control and experimental groups of rats

	Control group	Negative group	PcLG group	PcNCA group
TPC	18.14±1.14	207.12±8.45	180.55±9.83	160.89±3.51
BUN	1.60±0.05	0.54±0.049	0.76±0.13	0.92±0.025
Creatinine	1.36±0.052	0.73±0.044	0.84±0.093	1.01±0.40

Determination of oxidative stress parameters

STZ induction generates uncontrolled ROS and activates the scavenging system that results in hyperglycaemia and production of excessive free radicals sufficient to damage the lipid membrane and cellular death. The rise in lipid peroxidation level decreases the catalase (CAT) activities and glutathione (GSH) levels in pancreatic tissues which diminish the antioxidant protective ability of the enzymes and thus, promote the formation of ROS.

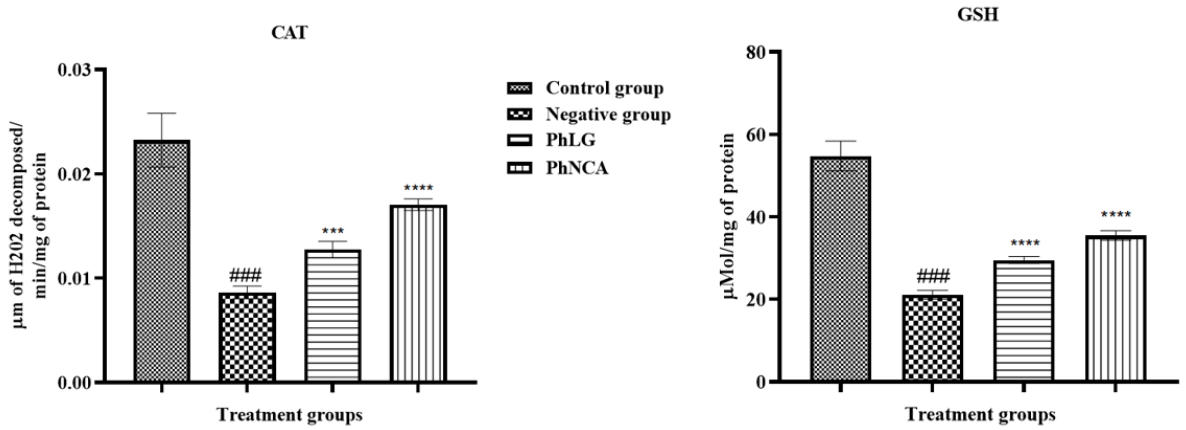

Figure 31. Effect of Pc and formulation PhConA on anti-oxidant parameters. (Mean ± S.E.M, ***p<0.001 and ***p<0.001 in comparison with diabetic control group. ###p<0.001 when the compared with the normal control group)

Histopathological analysis

The histopathological images of pancreas displayed an improvement in average number of Langerhan's islet cells in the animals administered with Pc and formulation PhConA in comparison to the negative group. STZ administration deteriorated the pancreatic beta cells that induced hyperglycaemic conditions with severe histopathological changes in the pancreatic tissues.

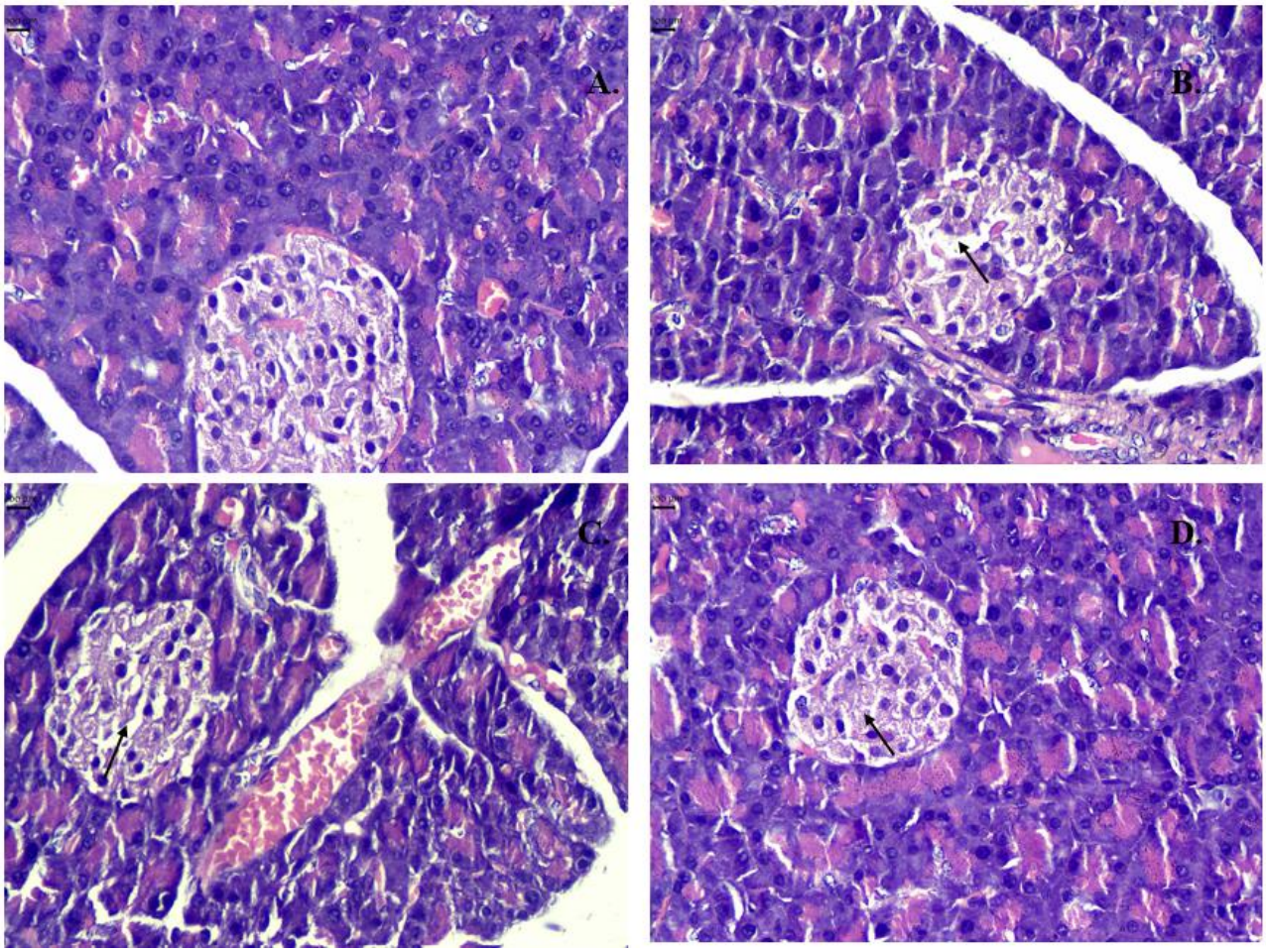

Figure 32. Histopathological images of the experimental animal's pancreas in anti-diabetic study of A. Normal group, B. Diabetic group, C. Diabetic + Pc-treated group and D. Diabetic + Formulation PhConA treated group

4. Preparation and characterization of metallic nanoparticles for STZ-induced diabetic rats

The present research work mainly involves synthesis of zinc-phthalocyanine nanoparticles, preparation of zinc-phthalocyanine-loaded PLGA-chitosan nanosystem and *in-vivo* efficacy study of the prepared system on streptozotocin-induced diabetic rats.

Methods

Synthesis of Zn-phthalocyanine nanoparticles (ZnPcN)

The zinc-phthalocyanine nanoparticles (ZnPcN) were prepared via pyrolysis with slight modification in the process as defined by Khitam et al.. For synthesis, 50 mL of 0.1 M solutions of zinc sulfate heptahydrate along with 100 mg of phthalocyanine was dispersed to 50 mL of 0.2 M NaOH and the sample was kept on continuous magnetic stirring at 100^{o}C for 12 h.

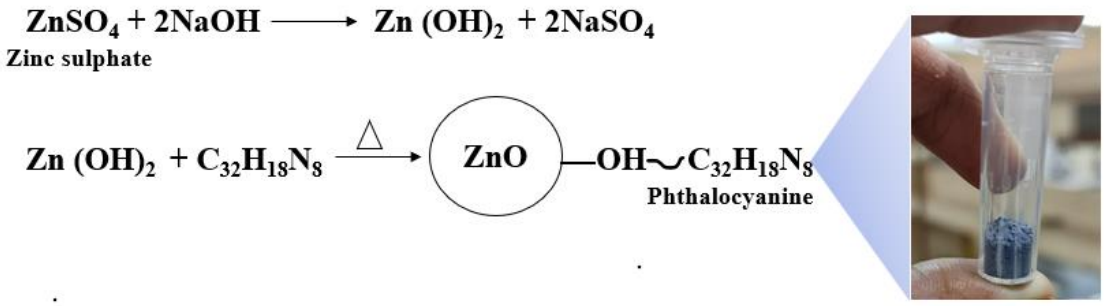

Preparation of ZnPcN-loaded PLGA nanoparticles (ZnPcPNs)

Central composite design (CCD)

The three-factor CCD was used to determine the importance of independent variables: PLGA (A), PVA (B) and chitosan (C) on 3 responses as particle size (R1), zeta potential (R2) and % entrapment efficiency (% EE). Twenty trials were obtained **(Table 1)** from CCD using Design Expert Software (Version 13, Trial, Stat-Ease Inc. Minneapolis, USA) and the formulation was optimized using response surface diagram. A quadratic model was selected on the significant results ($p < 0.05$), the least significant lack-of-fit and multiple correlation coefficients.

Formulation of ZnPcPNs

ZnPcPNs were prepared via nanoprecipitation method using different ratios of PLGA, chitosan and PVA as mentioned by the software **(Table 7)**. The organic system was prepared by dissolving a suitable amount of PLGA into DCM. Whereas for the preparation of aqueous phase, the required quantity of PVA along with chitosan dispersed in 1% v/v glacial acetic acid.

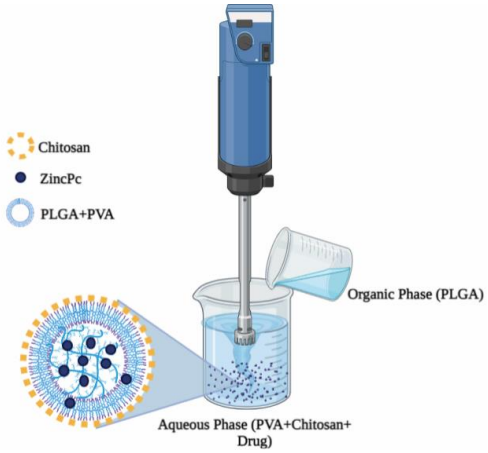

Figure 33. Preparation of ZincPc-loaded PLGA-chitosan nanoparticles

Table 7. Experimental design using central composite design

Run	Factor 1 A: PLGA (mg)	Factor 2 B: PVA (mg)	Factor 3 C: Chitosan (mg)
1	100	100	10
2	150	150	3.18207
3	150	150	20
4	65.9104	150	20
5	150	150	20
6	100	100	30
7	150	65.9104	20
8	100	200	30
9	150	150	20
10	200	100	30
11	150	234.09	20
12	150	150	20
13	150	150	20

14	150	150	36.8179
15	200	200	30
16	200	100	10
17	150	150	20
18	100	200	10
19	234.09	150	20
20	200	200	10

Results and discussion

The nanoprecipitation method was selected for the preparation of the nanoparticles, as the method is easily available and the scale-up is feasible. The DoE software was applied for the optimization of the formulation as it provides the critical amount required for the desired response along with the possible interaction of the selected factors on the obtained response.

Central composite design (CCD)

CCD design is a response surface method, considered more accurate and effective for building the quadratic model for the response variables. The obtained data as shown in Table 8. were fitted in various designs to optimize the best model which will define the connection between independent factors (PLGA, PVA and chitosan) and response (Particle size, zeta potential and % encapsulation efficiencies). The quadratic model was chosen as the best-fit model and the results showed that the independent variables significantly affected the a designated response as the P value>0.05.

Table 8. Response of particle size, zeta potential and % EE obtained from the different compositions of the variables

Run	Factor 1 A: PLGA mg	Factor 2 B: PVA mg	Factor 3 C: Chitosan mg	Response 1 Particle size nm	Response 2 Zeta potential mV	Response 3 % EE %
1	100	100	10	285.5	20.8	65.3
2	150	150	3.18207	298.5	-5.1	70.2
3	150	150	20	281.7	12.7	68.7
4	65.9104	150	20	203.5	22.5	68.1
5	150	150	20	281.7	12.7	68.7
6	100	100	30	350	27.5	66.5
7	150	65.9104	20	289.5	11.7	71.8
8	100	200	30	275.1	31.5	68.5
9	150	150	20	281.7	12.7	68.7
10	200	100	30	385.6	20.5	73.2
11	150	234.09	20	232.1	10.5	69.5
12	150	150	20	281.7	12.7	68.7
13	150	150	20	281.7	12.7	68.7
14	150	150	36.8179	310.5	30.5	71.9
15	**200**	**150**	**20**	**320.9**	**28.5**	**74.5**
16	200	100	10	405.1	-3.5	73.5
17	150	150	20	281.7	12.7	68.7
18	100	200	10	250.6	20.8	64.7
19	234.09	150	20	550.5	-5.5	78.4
20	200	200	10	335.6	-3.8	72.8

Influence of independent variables on particle size

In the present study, it was analysed that particle size of the nanoparticles produced was in range of 203.5- 550.5 nm. The best model was selected using ANOVA by calculating the F value and it was observed that the quadratic equation was considered the best-fit model. The results showed that the rise in the PLGA concentration along with chitosan produced larger size because with the higher PLGA concentration there is rise in the viscosity of organic system.

R1= +16.85+1.85*A-0.5784*B+0.0329*C-0.2689*AB-0.2068*AC+0.1054*BC+0.7635*A^2-0.2050* B^2+0.2647* C^2

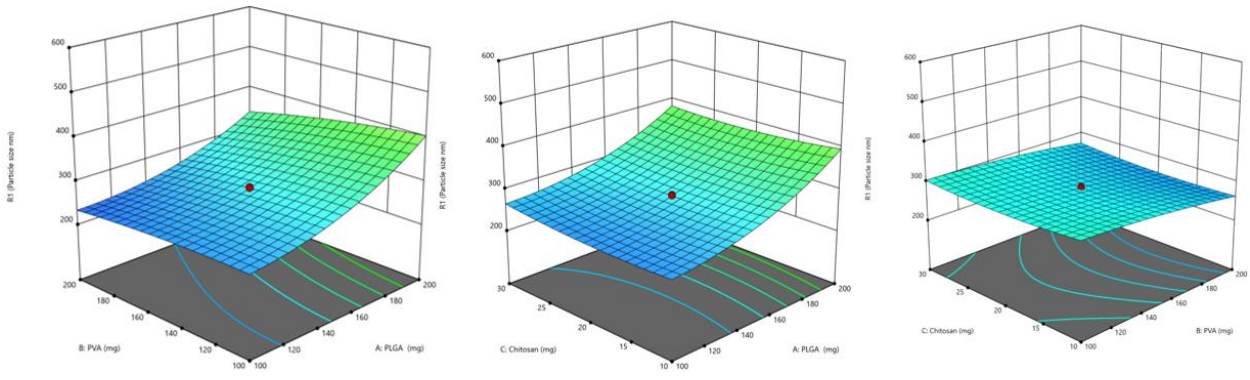

Figure 34. Influence of independent variables on particle size

Influence of independent variables on zeta potential

The zeta potential range for the obtained nanoparticles was in the range from -3.8 to +31.5 mV.

R2=+13.00-7.27*A+1.20*B+9.29*C-0.3750*AB+5.70*AC+2.37*BC-0.3257*A^2+0.5935* B^2+1.16* C^2

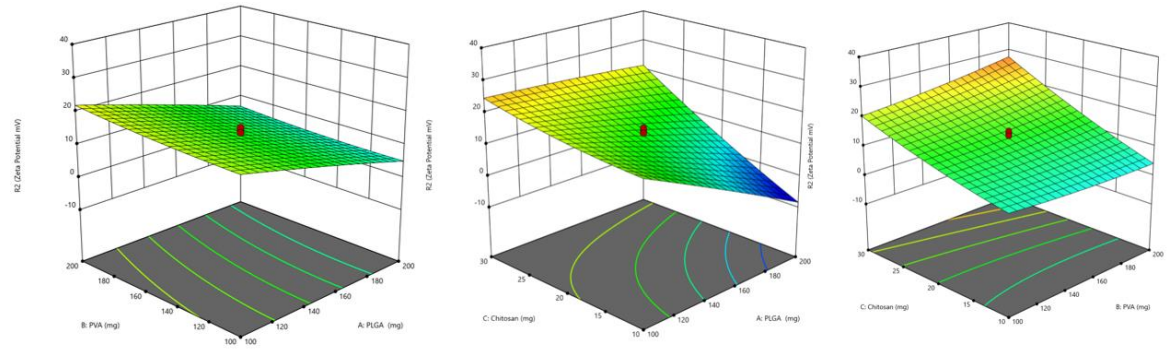

Figure 35. Influence of independent variables on zeta potential

Influence of independent variables on entrapment efficiency (%)

The entrapment efficiency of the nanosystem was in the range of 65 to 75 % as shown in Table 7. The results showed that as the concentration of PLGA increased in presence of chitosan, higher entrapment was attained as a higher amount of polymer increases the viscosity of the organic phase which lower the shear stress and produces nanoparticles of larger size.

R3= +1.84+0.0298*A-0.0003*B+0.0037*C-0.0017*AB-0.0021*AC+0.0046*BC

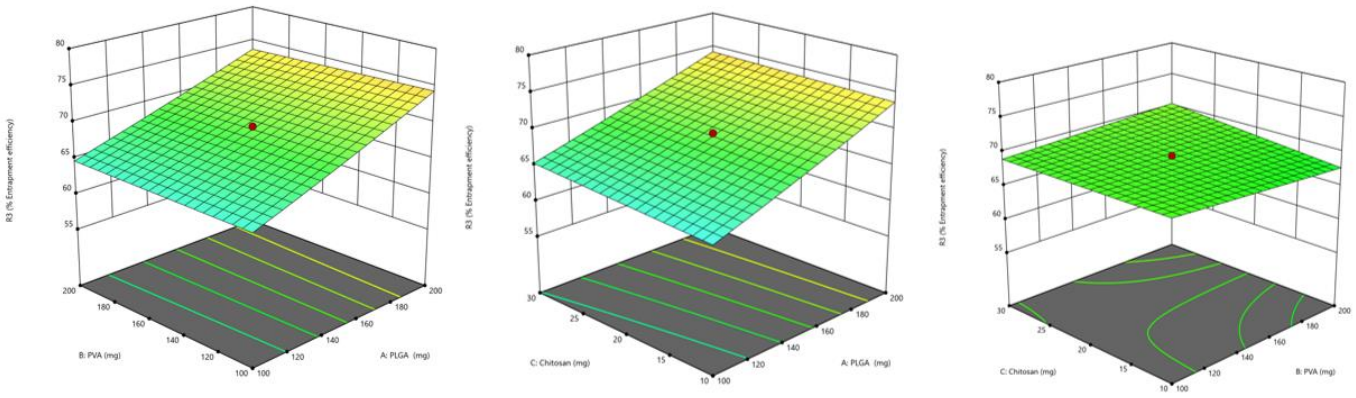

Figure 38. Influence of independent variables on entrapment efficiency (%)

Table 9. Results of ANOVA for quadratic response model

Responses	Sum of Squares	df	Mean square	F value	P value	R^2	Adjusted R^2	CV%
Y1	0.024	3	7.743	6.43	0.0075	0.8872	0.7857	5.12
Y2	0.073	3	0.028	7.96	0.0072	0.9210	0.8500	31.46
Y3	0.2878	3	1.253	4.674	0.0635	0.8325	0.7553	0.7583

Table 10. Validation of central composite design for formulation ZnPcPNs

Formulation composition Formulation ZnPcPNs			Predicted values			Experimental values		
X1	X2	X3	PS	ZP	EE	PS	ZP	EE
180.55	167.78	20.16	323.842	29.45	72.0073	335.6	27.87	75.67

Scanning Electron Microscopy (SEM)

The blank nanoparticles displayed smooth spherical surface with porous with uniform dispersion of particles. In case of formulation ZnPcPNs, majority of the nanoparticles appeared to be with smooth surfaces; however, the entrapment of the drug might have disturbed the circular shape of the nanoparticles.

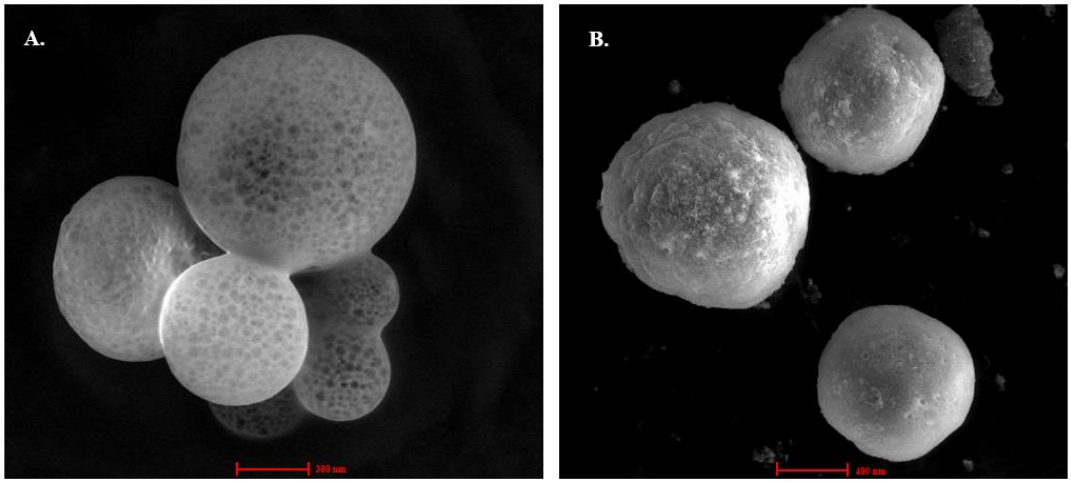

Figure 39. SEM images of A. Blank nanoparticles and B. Formulation ZnPcPNs

Transmission Electron Microscopy (TEM)

The TEM image of blank and ZnPcPNs formulations displayed effective coating of chitosan over the nanoparticles. The images show spherical-shaped molecules with a well-defined double walled-structure core-shell structure. The effective coating of chitosan could be visible due to the possible adsorption and binding of chitosan with the PLGA surface via hydrogen bond with protonated -NH groups of chitosan and -COOH groups of PLGA.

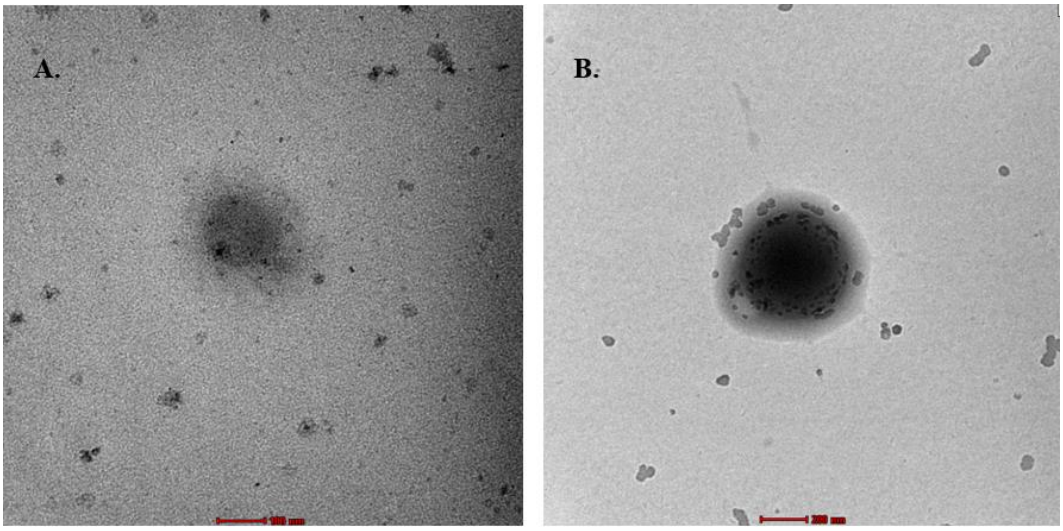

Figure 40. TEM images of A. Blank nanoparticles and B. Formulation ZnPcPNs

Fourier Transform Infrared Spectrophotometer (FTIR)

In case of ZnPc formation, the formation of newer peak at 750 cm^{-1} and intensification of the hydroxyl stretching vibration signifies the formation of C-H bending vibration and creation of newer bond of zinc and phthalocyanine.

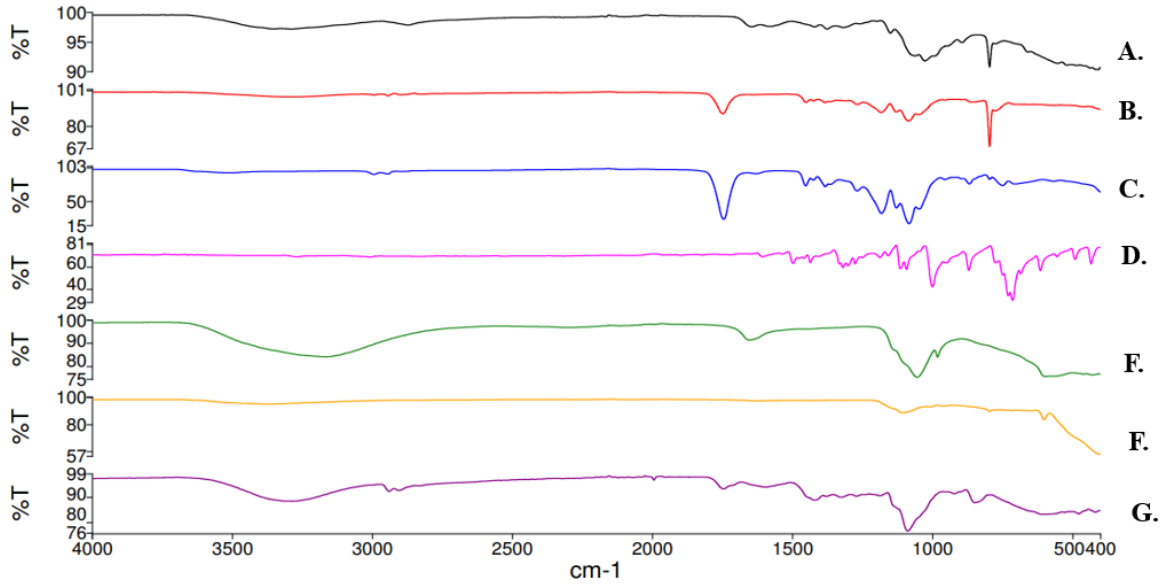

Figure 41. FTIR spectrum of A. Chitosan, B. PVA, C. PLGA, D. Phthalocyanine, E. PcZinc, F. Blank PLGA and G. formulation ZnPcPNs

X-Ray Diffraction (XRD)

The XRD pattern of ZnPcN, blank formulation and ZnPcPNs are demonstrated in figure 42. In case of ZnPcN, the predominant peaks observed were $2\theta^{o}$=6.74, 8.32, 14.64 and 25.7 along with weak peaks at 27. 28 and 46.24. According to Senthilarasu et al., such weak peaks indicate the nature of the molecular orientation of ZnPcN. The broad peak centered at 19. 38 indicates the significance of the amorphous nature of PLGA nanoparticles.

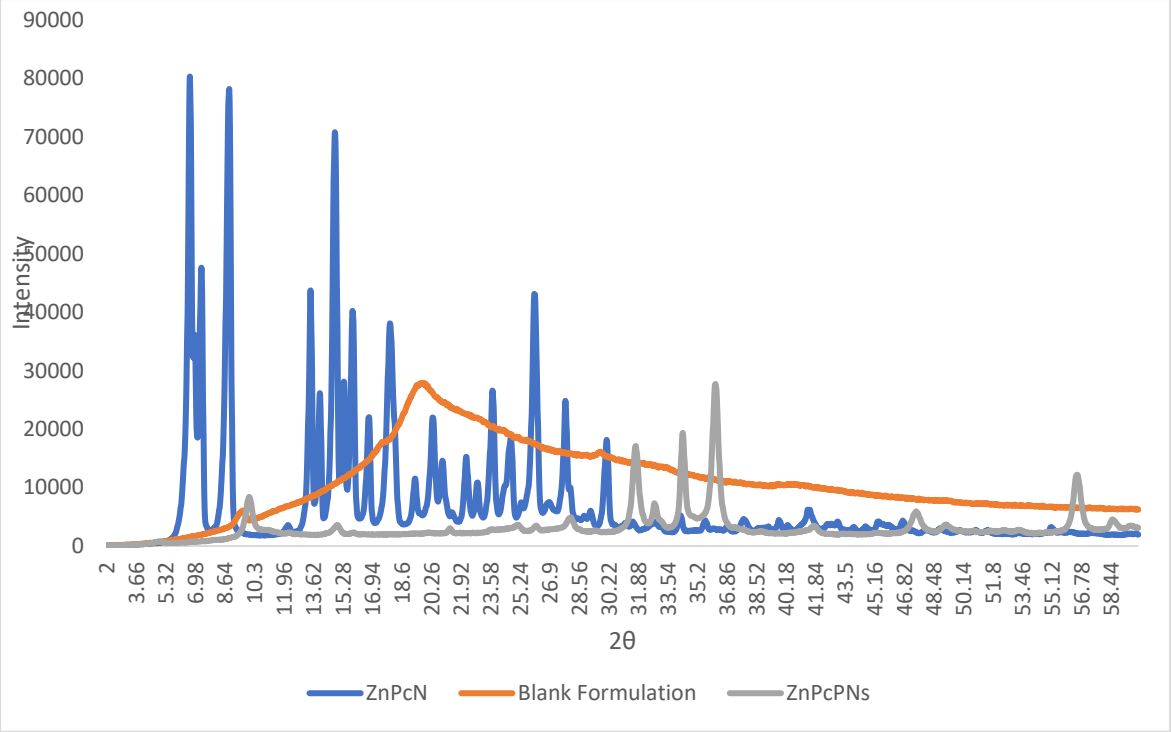

Figure 42. XRD pattern of ZnPcN, blank formulation and ZnPcNs

Differential scanning calorimetry (DSC)

The DSC of ZnPcN shows two small endothermic peaks 125^{o}C and 280^{o}C. According to Pajak et al., the endothermic peak for ZnPcN is observed at 88°C and 351°C due to the dehydration process and secondly due to the gradual mass loss. However, the peaks observed in the present ZnPcN curve may be due to the shift in peak during the loss of six water molecules of $ZnSO_4$ from 70-120^{o}C and another sample loss of SO_3 molecule.

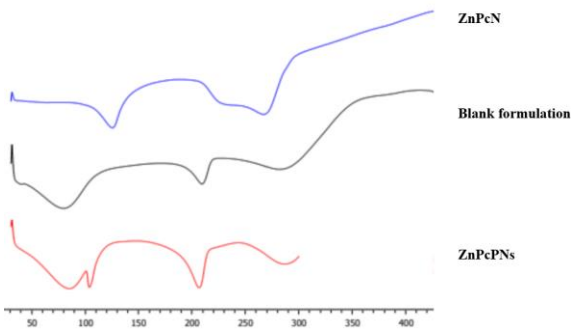

Figure 43. DSC curve of ZnPcN, Blank formulation and formulation ZnPcPNs

Controlled release study

The release of ZnPcN was carried in two pH: 1.2 (Gastric pH) and 6.8 (Intestinal pH) as shown in figure 44. The encapsulation of ZnPcN into the amorphous PLGA-chitosan nanoformulation proved to be effective for the release of the drug. The release study was carried out for 72 h and it was observed that 60.58±3.56% of encapsulated drug was released at pH 6.8 within 24 h however; only 29.58±1.37% was released at pH 1.2.

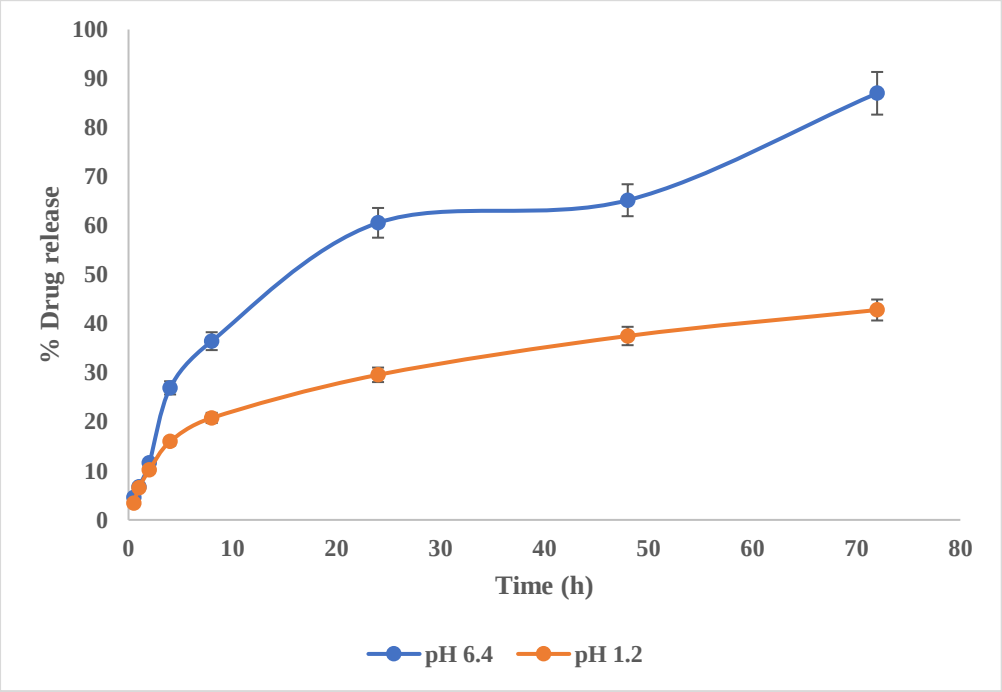

Figure 44. The release pattern of formulation ZnPcPNs in pH 1.2 and 6.4.

Animal study

Plasma analysis

Blood glucose level

Diabetes was induced in rats using streptozotocin (STZ) and the animals were treated with free PnZnN (daily) and formulation ZnPcPNs (once every three days). Blood glucose level was determined in the experimental animals at different time internal (0, 7, 14, 21and 28 days) after

the first dose of PnZnN and formulation ZnPcPNs administration as shown in figure 45. The entrapment of such a conjugated system into the chitosan PLGA network enhanced its diabetic activity by controlling the release of the drug in the disease condition state via oral route.

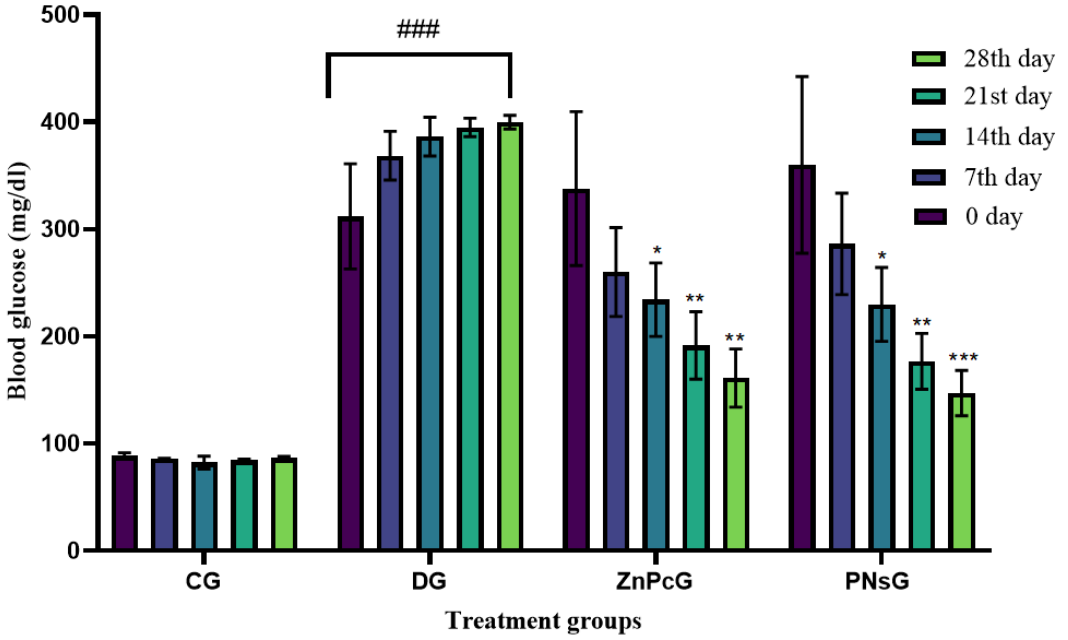

Figure 45. Glucose level profile of free drug and formulation ZnPcPNs. Results are expressed as mean ± S.D. of 7 observations in each case. ***p<0.001, **p<0.01 and *p<0.1 when compared with diabetic control group. ###p<0.001 when the diabetic control group compared with the normal control group.

Cholesterol, triglyceride and alkaline phosphatase (ALP)

From the cholesterol and triglycerides results it was observed that the levels were significantly higher in diabetic group as compared to the control group (p= 0.0023). STZ induction leads to improper functioning and metabolism of glucose that creates hypercholesterolemia and hypertriglyceridemia because of increase in cholesterol synthesis and intestinal absorption.

Table 9. Cholesterol and triglycerides level in diabetic animals

Groups	Cholesterol (mg/dL)	Triglyceride (mg/dL)	Alkaline phosphate (U/l)
CG	31.46±2.42	72.22±6.75	54.12±11.61
DG	77.80± 3.80	246.07±93.57	81.27±3.78
ZnPcG	53.84±2.76 [a]	86.05±7.92	75.6±6.78[a]
PNsG	39.14±2.06 [a]	81.27 ±51.39	67.81±19.67

Each value represents the mean ± SEM

[a] significant difference compared with controls in each column

Urine analysis

STZ is proposed to directly damage renal functioning predominantly the proximal renal tubule as it mainly resembles the aminoglycosides which are considered as a potential nephrotoxic antibody.

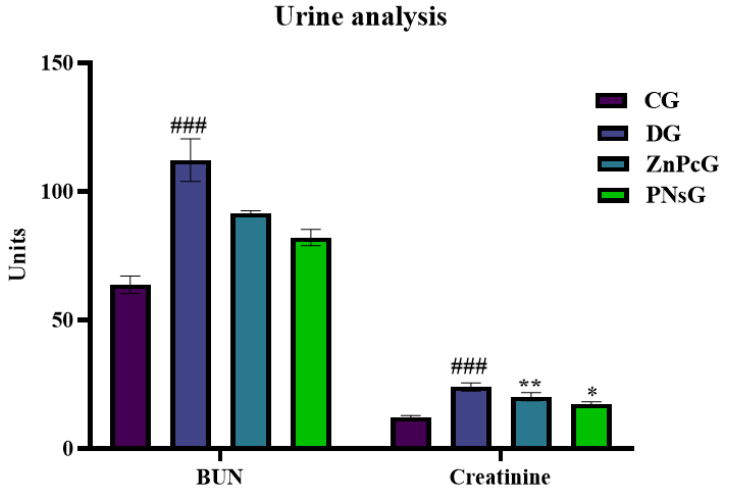

Figure 46. Urine analysis of diabetic animals. Results are expressed as mean ± S.D.*p<0.001, **p<0.01 and *p<0.1 when compared with diabetic control group. ###p<0.001 when the diabetic control group compared with the normal control group.**

TNF-alpha (TNF-α)

STZ-induced diabetes is associated with the rise in inflammatory cytokines like TNF-a and IL-6 which created pancreatic beta-cell apoptosis and other diabetic complications due to endothelial dysfunction.

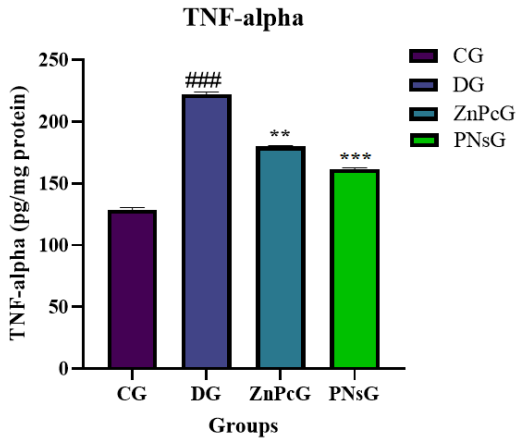

Figure 47. TNF-α levels in diabetic animals. Results are expressed as mean ± S.D.*p<0.001, **p<0.01 and *p<0.1 when compared with diabetic control group. ###p<0.001 when the diabetic control group compared with the normal control group.**

Histopathological analysis

Figure 48. represents the histopathological images of liver, kidney, and pancreas for control group, diabetic group, diabetic group treated with ZnPc, and diabetic group treated with ZnPcPNs. As shown in histopathological image of liver (figure 48 A), the control group animals possess normally aligned hepatocytes surrounded by central vein and separated by thin wall sinusoids spaces lined by von Kupffer cells. The untreated diabetic group (figure 48 B) displayed increase in the apoptotic hepatocytes along with distortion of hepatic lobules. The foci present in the diabetic rats illustrates the inflammatory cells infiltrate formed of lymphocytes and plasma. Figure 48 C. and D. represents well-arranged hepatocytes surrounded by major veins and sinusoidal spaces like the control group. The administration of PnZnN and

formulation ZnPcPNs might ameliorate damaged hepatic lobules with recovered cytoplasm and reduced residual inflammation considering the central vein and moderately dilated sinu.

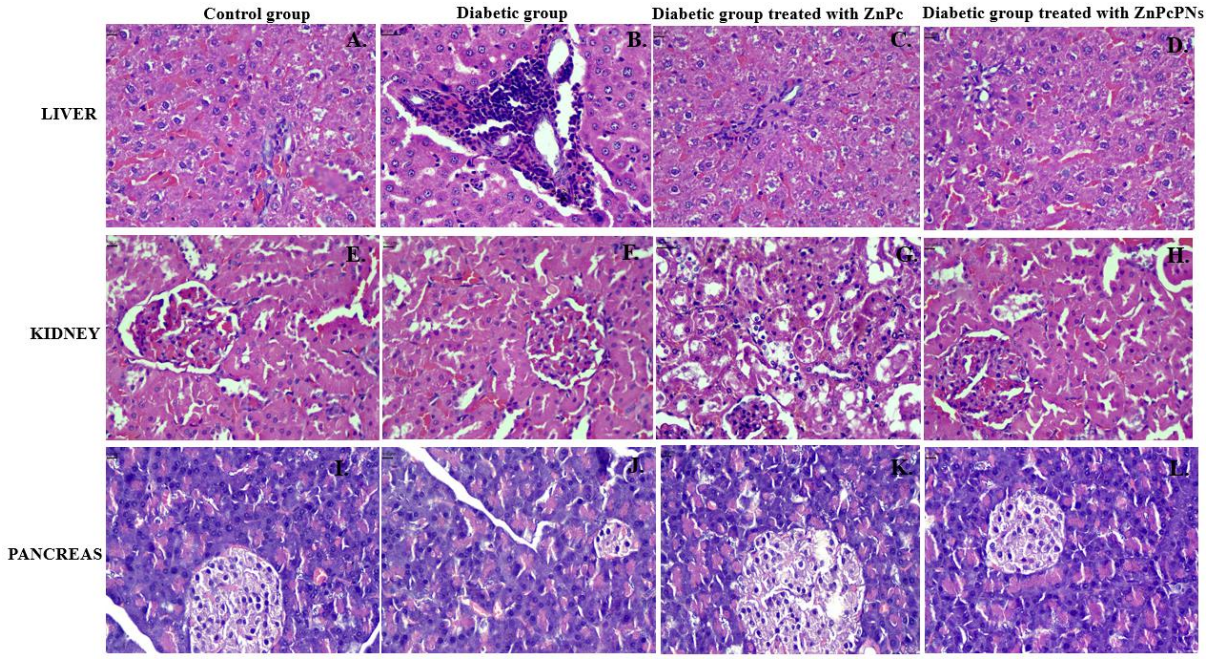

Figure 48. Histopathology examination of sections. A. Control liver, B. Diabetic liver, C. Diabetic group treated with ZnPc liver, D. Diabetic group treated with ZnPcNs liver, E. Control Kidney, F. Diabetic kidney, G. Diabetic group treated with ZnPc kidney, H. Diabetic group treated with ZnPcNs kidney, I. Control pancreas, J. Diabetic pancreas, K. Diabetic group treated with ZnPc pancreas and I. Diabetic group treated with ZnPcNs pancreas

5. Preparation and characterisation of nanotechnology-based biosensor strip for detection of diabetes from exhaled air

The objective of the present work is to prepare a non-invasive detection method for diabetes from exhaled air.

Biosensors are the devices which use for living organism or biological molecules, especially enzymes or antibodies, to detect the presence of chemicals in the biofluids. In order to maintain

normal blood glucose levels, biosensors emerge as a tool for continuous monitoring of blood glucose. The conventional biosensors are invasive, expensive and lack of sensitivity for accurate detection. Application of nanotechnology in biosensor will help for higher specificity, accuracy and sensitivity. Breath acetone has been shown to have strong correlation with blood glucose level. The acetone concentration in the breath varies from 300 to 900 ppb in healthy people to more than 1800 ppb in individuals with diabetes.

Method

For the preparation of the nanotechnology-based biosensor strip, 4 mL of ethylenediame with 4 mL of methamethyl acrylate and 400 mg of sodium nitroprusside were mixed. Further, 4 mL Ethylenediame and 4 mL of methamethyl acrylate were added again and this led to the formation of G1 generation. For the preparation of strip, the strip was firstly coated with NaOH and later with nanoparticles to detect the colour change.

Results and discussion

FTIR

It can be seen from that, compared with the 1.0 G sample, the 1.0 G PAMAM–sodium nitroprusside conjugate possesses absorption bands broadening at 3314 cm1 due to stretching vibration of the O–H bond, bands at 1564 and 1469 cm1 due to the aromatic (C-C) stretching vibration, strong bands at 1642 cm1 due to the aromatic amide (–CONH2) and shifting of the C–H stretching from 2919 and 2852 to 2973 and 2884 cm1.

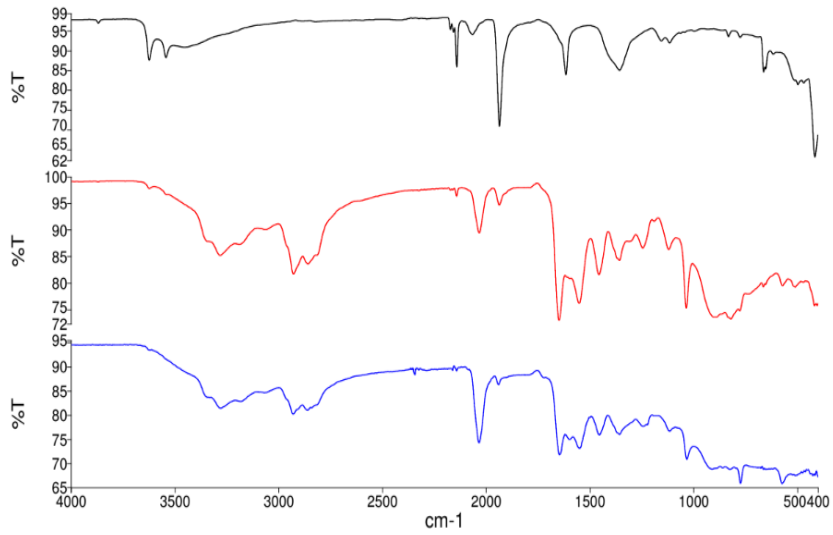

Figure 49. FTIR spectrum of A. Sodium nitroprusside, B. Blank dendrimer, C. Sodium nitroprusside-loaded dendrimers

SEM analysis

In this figure, nitroprusside-loaded dendrimers demonstrated the formation of spherical structure. The figure also shows that nitroprusside-loaded dendrimers dispersion is uniformly distributed and embedded on filter paper.

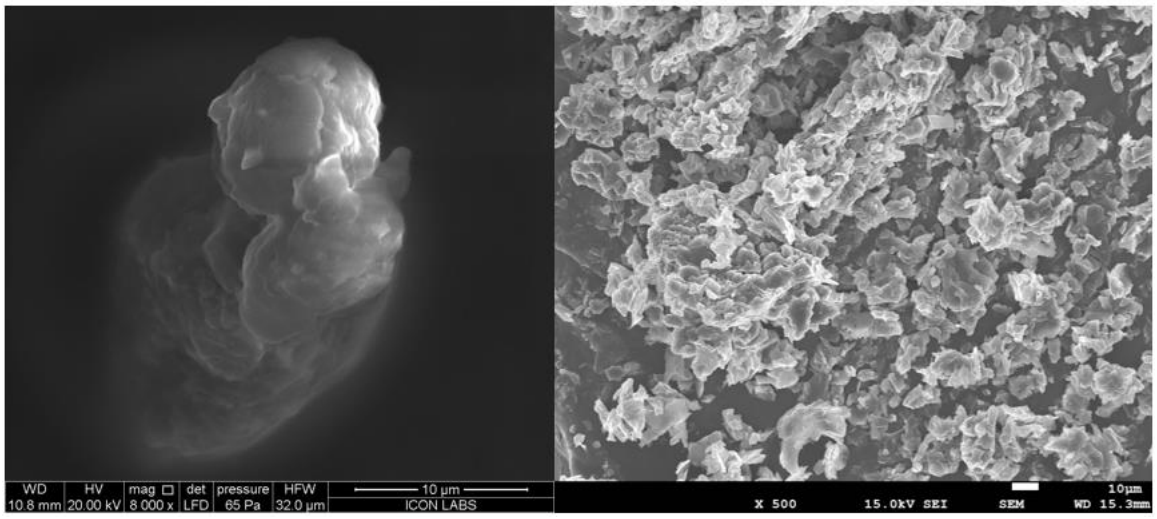

Validation of paper strip

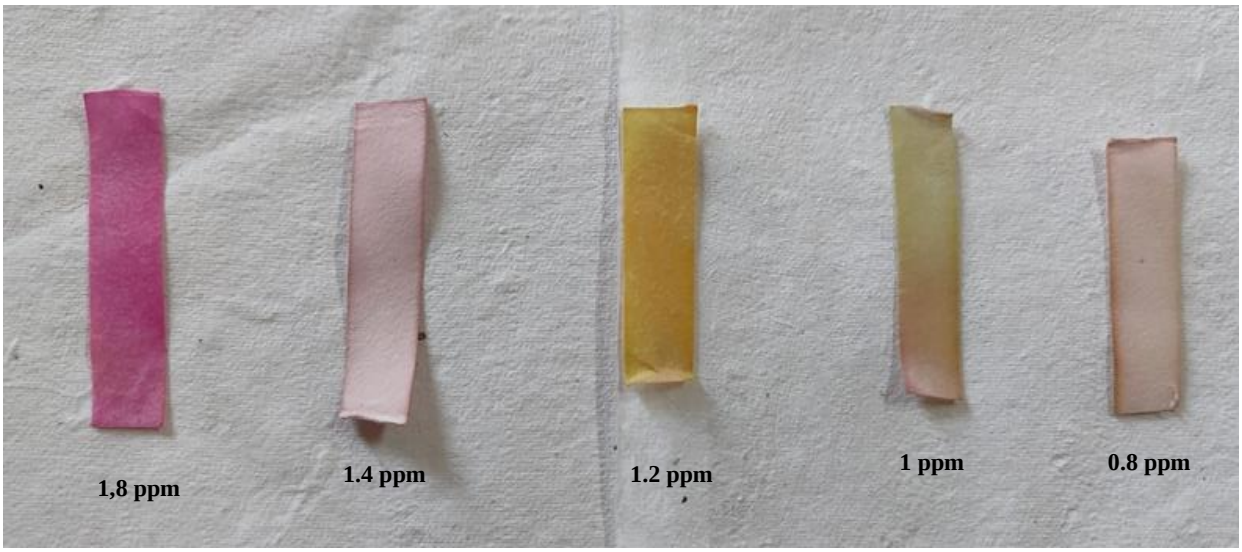

The increase of acetone concentration led to the colour change. The change in the concentration showed the colour change from light yellow to pink.

HSV model

The graph was plotted for each H, S and V of the color change against different concentration of acetone in ppb level of paper strip.

For color analysis Hue- Saturation-Value (HSV) color model was used in which hue (H) value of color refers to the pure color that is resembled. Hence all the shades and tints of pink have same hue. Saturation (S) of a color describes whiteness of color. Saturation of standard pink color is 100% and that of white color is 0%.

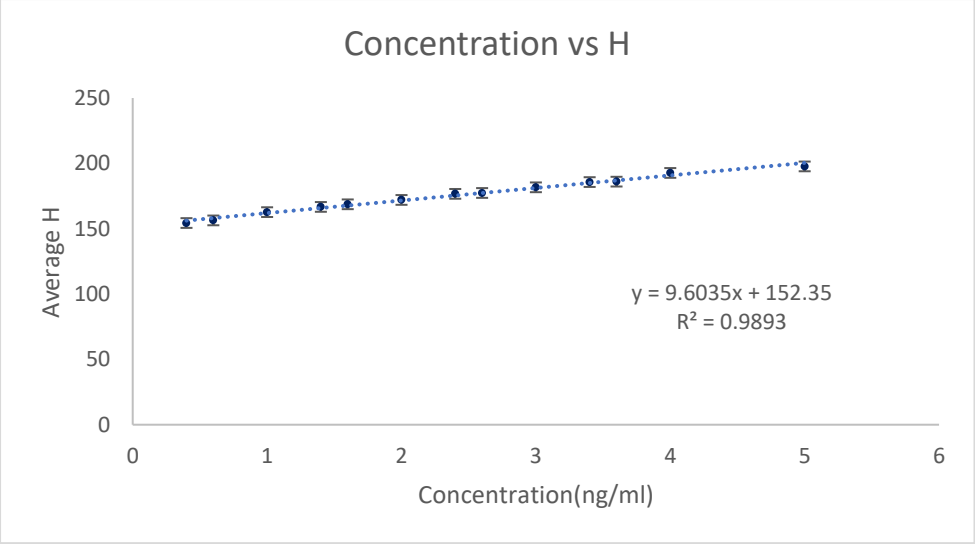
Concentration vs H
Average H
250
200
150
100
50
0
0
1
2
3
4
5
6
Concentration(ng/ml)
y = 9.6035x + 152.35
R² = 0.9893

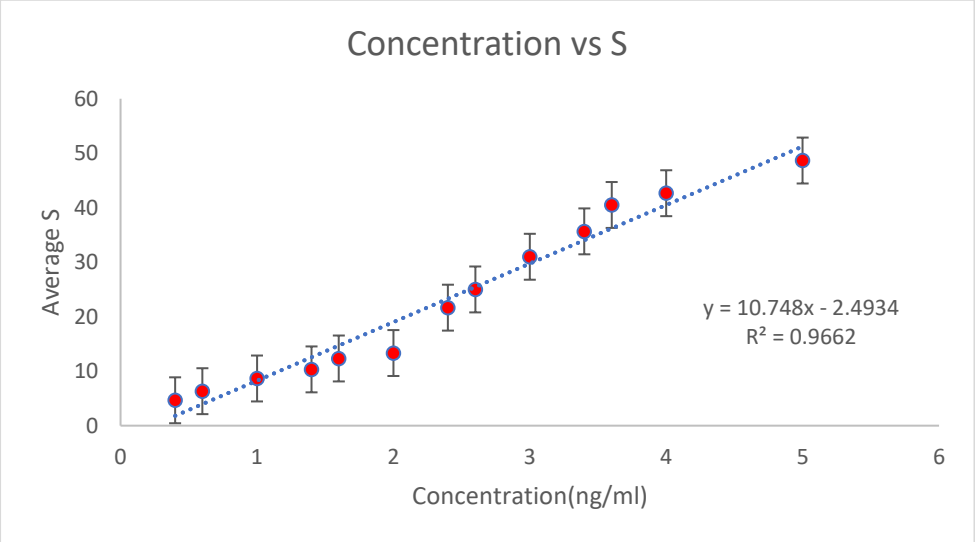
Concentration vs S
Average S
60
50
40
30
20
10
0
0
1
2
3
4
5
6
Concentration(ng/ml)
y = 10.748x - 2.4934
R² = 0.9662

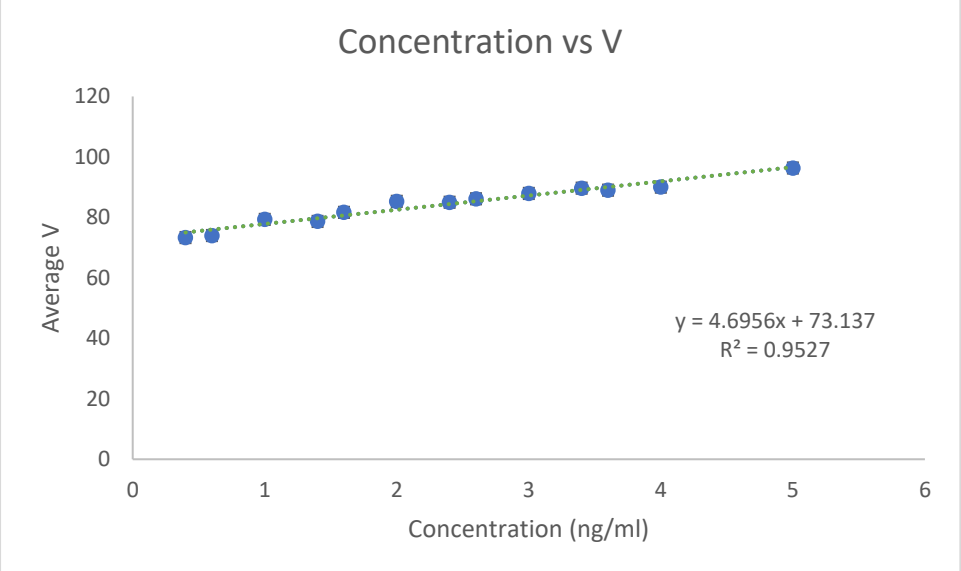
Concentration vs V
Average V
120
100
80
60
40
20
0
0
1
2
3
4
5
6
Concentration (ng/ml)
y = 4.6956x + 73.137
R² = 0.9527

Moreover, no color changes were observed in presence of other gas and mean S values obtained were significantly lower than the values in linearity range which confirmed that the developed system is specific for acetone only.

Conclusions

Phthalocyanine diabetic activity was proved to be effective for the period of 28 days with decrease in the hyperglycaemic, hyperlipidaemic and oxidative damage parameters. The polymeric, lipid and metallic nanoparticles were synthesized and its activity was proved in STZ-induced diabetic rats. Polymeric and lipid nanoparticles were administered via *I.V* route whereas metallic nanoparticles via oral route and their activity was able to decrease the hyperglycaemic and hyperlipidaemic effect in the diabetic rats. Moreover, the anti-oxidant activity of phthalocyanine was increased after entrapment into the nanocarrier systems as it was able to prevent the ROS damage. The biosensor was able to detect the diabetic condition via addressing the presence of acetone.

Outcome

Publications

Authors	**Title**	**Type of manuscript**	**I.F.**	**Status**
Review article				
Sharayu Govardhane; Pravin Shende	Orientation of nanocarriers in subarachnoid space: A tweak in strategic transport for effective CNS delivery	Review article	5.062	Published
Sharayu Govardhane; Pravin Shende	"Integration of green nanotechnology with silica for corrosion inhibition." Corrosion Reviews 39.3 (2021): 211-218.	Review article	3.690	Published

Research articles				
Sharayu Govardhane; Pravin Shende	"Colloidal complexed nanocarriers: A modulated aspect in fabrication and characterization for streptozotocin-induced diabetic rats." Colloids and Surfaces A: Physicochemical and Engineering Aspects (2022): 129755.	Research article	5.518	Published
Sharayu Govardhane; Pravin Shende	"Potential of phthalocyanine on streptozotocin-induced diabetic rats: An initiative of dye in substitution of therapeutics." Journal of Porphyrins and Phthalocyanines 26.10 (2022): 664-671.	Research article	1.914	Published
Sharayu Govardhane; Pravin Shende	Phthalocyanine-based glucose-responsive nanocochleates for dynamic prevention of β-cell damage in diabetes	Research article	5.586	Revision received
Sharayu Govardhane; Pravin Shende	Zinc-conjugated phthalocyanine PLGA nanoparticles for diabetes	Research article	-	Ready for communication

Book chapters

Sharayu Govardhane; Pravin Shende	"Strategies-Based Intrathecal Targeted Drug Delivery System for Effective Therapy, Modeling, and Controlled Release Action." Modeling and Control of Drug Delivery Systems. Academic Press, 2021. 213-225.	Book chapter	-	Published

Sharayu Govardhane; Pravin Shende	"Polymeric-Ceramic Nanocomposites Toxicity." Handbook of Polymer and Ceramic Nanotechnology. Cham: Springer International Publishing, 2021. 723-742.	Book chapter	-	Published
Govardhane, Sharayu, Sahil Gandhi, and Pravin Shende.	"Neural-ensemble-based detection: a modern way to diagnose lung cancer." Artificial Intelligence in Cancer Diagnosis and Prognosis, Volume 1: Lung and kidney cancer. IOP Publishing, 2022.	Book chapter	-	Published

Conference

Sharayu Govardhane; Pravin Shende	MIP-based nanosponges for entrapment of cholesterol in FaSSIF-C	4th European Conference on Pharmaceutics, France	20^{th}-21^{st} March, 2023	Applied for funding

Patent

Sharayu Govardhane; Pravin Shende	NANOTECHNOLOGY-BASED APPROACH FOR DETECTION OF DIABETES FROM EXHALED AIR.	Provisional patent	Docket Number:12926

References

1. American Diabetes Association. Diagnosis and classification of diabetes mellitus. Diabetes Care. 2009;32 Suppl 1(Suppl 1):S62-S67. Doi:10.2337/dc09-S062
2. Saeedi P, Petersohn I, Salpea P, Malanda B, Karuranga S, Unwin N, Colagiuri S, Guariguata L, Motala AA, Ogurtsova K, Shaw JE, Bright D, Williams R; IDF Diabetes Atlas Committee. Global and regional diabetes prevalence estimates for 2019 and

projections for 2030 and 2045: Results from the International Diabetes Federation Diabetes Atlas, 9th edition. Diabetes Res Clin Pract. 2019; 157:107843. Doi: 10.1016/j.diabres.2019.107843.

3. Report of the Expert Committee on the Diagnosis and Classification of Diabetes Mellitus. Diabetes Care. 1997 Jul;20(7):1183-97. Doi: 10.2337/diacare.20.7.1183.
4. Wright E Jr, Scism-Bacon JL, Glass LC. Oxidative stress in type 2 diabetes: the role of fasting and postprandial glycaemia. Int J Clin Pract. 2006;60(3):308-314. Doi:10.1111/j.1368-5031.2006.00825.x
5. https://diabetes.diabetesjournals.org/content/66/2/241
6. Asif M. The prevention and control the type-2 diabetes by changing lifestyle and dietary pattern. J Educ Health Promot. 2014;3:1. Doi:10.4103/2277-9531.127541.
7. Saasa V, Malwela T, Beukes M, Mokgotho M, Liu CP, Mwakikunga B. Sensing Technologies for Detection of Acetone in Human Breath for Diabetes Diagnosis and Monitoring. Diagnostics (Basel). 2018; 8(1):12. Doi: 10.3390/diagnostics8010012.
8. Zhang Y, Lovell JF. Recent applications of phthalocyanines and naphthalocyanines for imaging and therapy. Wiley Interdiscip. Rev. Nanomed. 2017;9(1):10. Doi:10.1002/wnan.1420.
9. Melo MAB, Caetano W, Oliveria EL, Barbosa PM, Rando ALB, Pedrosa MMD, Godoi VAF. Effects of nanoparticles of hydroxy-aluminum phthalocyanine on markers of liver injury and glucose metabolism in diabetic mice. Braz J Med Biol Res. 2019; 52(1): e7715. Doi: 10.1590/1414-431X20187715.
10. Siddiqui SA, Or Rashid MM, Uddin MG, Robert MO, Uddin G, Robel F, Hossain SM, Haque A, Jakaria. Biological efficacy of zinc oxide nanoparticles against diabetes: a preliminary study conducted in mice. Biosci Rep. 2020; 40(4):BSR20193972. Doi: 10.1042/BSR20193972.

11. Souto EB, Souto SB, Campos JR, Severino P, Pashirova TN, Zakharova LY, Silva AM, Durazzo A, Lucarini M, Izzo AA, Santini A. Nanoparticle Delivery Systems in the Treatment of Diabetes Complications. Molecules (Basel, Switzerland), 2019; 24(23), 4209. Doi: 10.3390/molecules24234209.
12. Dizaj SM, Jafari S, Khosroushahi AY. A sight on the current nanoparticle-based gene delivery vectors. Nanoscale Res Lett. 2014; 9(1):252. Doi: 10.1186/1556-276X-9-252.
13. ünsel A, Alici EH, Bilgiçli AT, Arabaci G and Yaraşir MN. *Turkish J. Chem.* 2019; **43**: 1030-1039.
14. Rahimi-Madiseh M, Malekpour-Tehrani A, Bahmani M and Rafieian-Kopaei M. *Asian Pac. J. Trop. Med.* 2016; **9**: 825-831.
15. Shichiri M, Yoshida Y and Niki E. Unregulated Lipid Peroxidation in Neurological Dysfunction. Elsevier Inc.; 2014.
16. S. Allahyari, H. Valizadeh, L. Roshangar, M. Mahmoudian, F. Trotta, F. Caldera, M. Jelvehgari, P. Zakeri-Milani, Preparation and characterization of cyclodextrin nanosponges for bortezomib delivery, Expert Opin. Drug Deliv. 17 (2020) 1807–1816. https://doi.org/10.1080/17425247.2020.1800637.
17. M. Mihailiasa, F. Caldera, J. Li, R. Peila, A. Ferri, F. Trotta, Preparation of functionalized cotton fabrics by means of melatonin loaded β-cyclodextrin nanosponges, Carbohydr. Polym. 142 (2016) 24–30. https://doi.org/10.1016/j.carbpol.2016.01.024.
18. S. Torne, S. Darandale, P. Vavia, F. Trotta, R. Cavalli, Cyclodextrin-based nanosponges: effective nanocarrier for tamoxifen delivery., Pharm. Dev. Technol. 18 (2013) 619–625. https://doi.org/10.3109/10837450.2011.649855.
19. M. Fadel, K. Kassab, D.A. Fadeel, Zinc phthalocyanine-loaded PLGA biodegradable nanoparticles for photodynamic therapy in tumor-bearing mice, (2010) 283–292. https://doi.org/10.1007/s10103-009-0740-x.

20. Hollander, A. and Danino, D., 2015. Cochleate characterization by cryogenic electron microscopy methods: Cryo-TEM and Cryo-SEM. Colloids and Surfaces A: Physicochemical and Engineering Aspects, 483, 187–192.
21. Hurkat, P., Jain, A., Jain, A., Shilpi, S., Gulbake, A., and Jain, S.K., 2012a. Concanavalin a conjugated biodegradable nanoparticles for oral insulin delivery. Journal of Nanoparticle Research, 14 (11).
22. Hurkat, P., Jain, A., Jain, A., Shilpi, S., Gulbake, A., and Jain, S.K., 2012b. Concanavalin a conjugated biodegradable nanoparticles for oral insulin delivery. Journal of Nanoparticle Research, 14 (11), 1–15.
23. Jiang, T., Huang, Z., Lin, Y., Zhang, Z., Fang, D., and Zhang, D.D., 2010. The protective role of Nrf2 in streptozotocin-induced diabetic nephropathy. Diabetes, 59 (4), 850–860.
24. Govardhane S, Shende P. Potential of phthalocyanine on streptozotocin-induced diabetic rats: An initiative of dye in substitution of therapeutics. J Porphyr Phthalocyanines. 2022;26(10):664–71.
25. Hirenkumar M, Steven S. Poly Lactic-co-Glycolic Acid (PLGA) as Biodegradable Controlled Drug Delivery Carrier. Polymers (Basel). 2012;3(3):1–19.
26. Liu Y, Wu X, Mi Y, Zhang B, Gu S, Liu G, et al. PLGA nanoparticles for the oral delivery of nuciferine: Preparation, physicochemical characterization and in vitro/in vivo studies. Drug Deliv. 2017;24(1):443–51.
27. Li Z, Tao W, Zhang D, Wu C, Song B, Wang S, et al. The studies of PLGA nanoparticles loading atorvastatin calcium for oral administration in vitro and in vivo. Asian J Pharm Sci. 2017;12(3):285–91.

28. Kumar G, Shafiq N, Malhotra S. Drug-loaded PLGA nanoparticles for oral administration: Fundamental issues and challenges ahead. Crit Rev Ther Drug Carrier Syst. 2012;29(1):149–82.

Candidate **Supervisor**

Ms. Sharayu Govardhane **Dr. Pravin K. Shende**